

UCLA

UCLA Electronic Theses and Dissertations

Title

Accelerating the Development of Diagnostic Biomarkers and Mitigating Drugs for Radiation Injury with Quantitative Mass Spectrometry

Permalink

<https://escholarship.org/uc/item/5sf7q3n7>

Author

Liu, Kate

Publication Date

2019

Peer reviewed|Thesis/dissertation

UNIVERSITY OF CALIFORNIA

Los Angeles

**Accelerating the Development of Diagnostic Biomarkers and Mitigating Drugs for
Radiation Injury with Quantitative Mass Spectrometry**

A dissertation submitted in partial satisfaction
of the requirements for the degree Doctor of Philosophy
in Chemistry

by

Kate Liu

2019

ABSTRACT OF THE DISSERTATION

Accelerating the Development of Diagnostic Biomarkers and Mitigating Drugs for Radiation Injury with Quantitative Mass Spectrometry

by

Kate Liu

Doctor of Philosophy in Chemistry

University of California, Los Angeles, 2019

Professor Joseph Ambrose Loo, Chair

Nuclear and radiological terrorism is an on-going public health concern, but very few effective measures exist to assess the extent of the injury or counter the injuries from these potential attacks. In response to this need, the UCLA Center for Medical Countermeasures against Radiation (CMCR) has dedicated their research efforts on radiation biodosimetry and drug development. On the diagnostic side, existing biodosimetry is only able to provide a crude estimate of radiation exposure dose. More effective diagnostic tools are needed to confirm exposure and predict tissue-specific radiation injury progression. Towards this end, we aimed to develop protein biomarkers that can assess organ-specific radiation damage. Utilizing quantitative mass spectrometry (MS)-based proteomics, we performed discovery experiments to identify proteins that have desirable biomarker characteristics. In addition, we evaluated a set of hypothesized biomarker candidates as part of antioxidant response using a targeted MS method. On the treatment side, very few medical products are available to mitigate radiation-induced injury. In fact, only three radiomitigators, through drug repurposing, have been approved by the FDA for treatment of hematopoietic acute radiation syndrome (H-ARS). The UCLA CMCR has

recently identified a novel group of small molecules from high throughput screening (HTS) for inhibitors of radiation-induced apoptosis. The lead compound dramatically decreases mortality from H-ARS in mice. To elucidate the mechanism of action for the lead compound, we utilized an emerging target identification approach based on thermal stability shift upon ligand binding (i.e. thermal proteome profiling or TPP). Data from TPP experiments proposed hypothetical targets for the lead compound, which can later be validated by protein-ligand binding studies and other means.

The dissertation of Kate Liu is approved.

James Akira Wohlschlegel

Anne M. Andrews

Joseph Ambrose Loo, Committee Chair

University of California, Los Angeles

2019

TABLE OF CONTENTS

ABSTRACT OF DISSERTATION.....	ii
Table of Contents.....	v
List of Figures and Tables.....	vii
Acknowledgements.....	ix
Biographical Sketch.....	xi
Chapter 1: Current status on medical preparedness for unexpected radiation exposure	1
Chapter 2: Discovery of new organ-specific biomarkers for radiation injury assessment	5
2.1 Abstract.....	5
2.2 Introduction.....	6
2.3 Materials and Methods.....	7
2.4 Results and Discussion.....	11
2.5 Conclusion.....	23
Chapter 3: Evaluation of biomarker potential of Nrf2-modulated antioxidant response proteins	24
3.1 Abstract.....	24
3.2 Introduction.....	25
3.3 Materials and Methods.....	29
3.4 Results and Discussion.....	34
3.5 Conclusion.....	44
Chapter 4: Target identification of novel radiation mitigators in development	47
4.1 Abstract.....	47
4.2 Introduction.....	49

4.3 Materials and Methods	59
4.3.1 Conventional TPP experiment	59
4.3.2 PISA TPP experiment	63
4.4 Results and Discussion	67
4.4.1 Results from conventional TPP experiment	67
4.4.2 Results from PISA TPP experiment	72
4.5 Conclusion	80
References	82

LIST OF FIGURES AND TABLES

Figure 2.1	13
Figure 2.2	14
Figure 2.3	15
Figure 2.4	15
Figure 2.5	17
Figure 2.6	17
Table 2.1	18
Table 2.2	19
Figure 2.7	20
Table 2.3	21
Table 2.4	22
Table 3.1	31
Figure 3.1	35
Figure 3.2	37
Figure 3.3	37
Figure 3.4	38
S3.1	46
Figure 4.1	50
Figure 4.2	51
Figure 4.3	52
Figure 4.4	54
Figure 4.5	55
Figure 4.6	56
Figure 4.7	57
Figure 4.8	58
Figure 4.9	59
Table 4.1	68

Table 4.2	68
Figure 4.10	69
Figure 4.11	70
Figure 4.12	71
Figure 4.13	72
Figure 4.14	72
Table 4.3	73
Figure 4.15	74
Figure 4.16	74
Figure 4.17	75
Figure 4.18	77
Figure 4.19	78
Figure 4.20	79
Table 4.4	79
Table 4.5	80

ACKNOWLEDGEMENTS

I would like to first thank my advisor, Dr. Joseph A. Loo, and Dr. Rachel R. Ogorzalek Loo, for their guidance and support throughout my PhD training. Their kindness and patience encourages many interdisciplinary collaborations and discussions. I am grateful for involvement in a broad scope of research projects and themes.

Being part of Loo lab family, I enjoyed the atmosphere fostered by past and present Loo lab members. I especially like to thank Hong Nguyen, Huilin Li, Sean Shen, Reid O'Brien Johnson, Pete Wongkongkathap, and Dyna Shirasaki, who helped me in the early days of my PhD and encouraged me to reach higher. I am also thankful to current lab members for their positive energy and curiosity both in and out of the lab.

I would like to thank Dr. Julian Whitelegge for the opportunity to work collaboratively on radiation biomarker and mitigation projects. I appreciate his guidance on project background and experimental directions. I would also like to thank Dr. William McBride for his guidance and expertise in radiation biology. I appreciate the mouse work performed by Elizabeth Singer in the biomarker projects. I am thankful for many other researchers who provided me with the cells for the target identification project including Dr. Ewa Micewicz and Christine Nguyen from Dr. McBride's lab, and Constance Yuen from Robert Damoiseaux's lab. Lastly, I would like to thank Dr. James Wohlschlegel, William Barshop, and Yasaman Jami for their help and instrument support for the thermal proteome profiling project.

I would like to acknowledge National Institutes of Health for the financial support for these projects. I am also thankful for the Natural Sciences and Engineering Research

Council of Canada (NSERC) for granting me the postgraduate scholarship for 4 years of my PhD.

Last, I am particularly thankful for my parents, for their encouragement and support throughout this PhD journey.

BIOGRAPHICAL SKETCH

EDUCATION

University of British Columbia, Vancouver, BC, Canada

B.Sc. with Distinction, Honors Chemistry, 2013

Thesis title: Reversible Modification of Quantum Dot with Peptides and DNAs for FRET-based Biosensing

Supervisor: Russ Algar

AWARDS AND HONORS

- Canadian NSERC Postgraduate Scholarship, 2016-2019
- US HUPO Student Travel Award, 2017

PUBLICATIONS

- [1] K. Liu, E. Singer, W. Cohn, E. D. Micewicz, W. H. McBride, J. P. Whitelegge, J. A. Loo. "Time-Dependent Measurement of Nrf2-Regulated Antioxidant Response to Ionizing Radiation towards Identifying Potential Protein Biomarkers for Acute Radiation Injury," *Proteomics-Clinical Applications*. Accepted for publication.
- [2] R. A. Warmack, H. Shawa, K. Liu, K. Lopez, L. Ding, J. A. Loo, J. Horwitz, S. G. Clarke. "The L-isoaspartate modification within protein fragments in the aging lens can promote protein aggregation," *Journal of Biological Chemistry*. Accepted for publication.
- [3] K. Lohnes, N. Quebbemann, K. Liu, F. Kobzeff, J. A. Loo, and R. R. Ogorzalek Loo, "Combining High-throughput MALDI-TOF Mass Spectrometry and Isoelectric Focusing Gel Electrophoresis for Virtual 2D Gel-based Proteomics.," *Methods*, Jan. 2016.
- [4] C.-C. Zhang, R. Li, H. Jiang, S. Lin, J. C. Rogalski, K. Liu, and J. Kast, "Development and Application of a Quantitative Multiplexed Small GTPase Activity Assay Using Targeted Proteomics," *J. Proteome Res.*, vol. 14, no. 2, pp. 967–976, Feb. 2015.
- [5] E. Petryayeva, R. Bidshahri, K. Liu, C. A. Haynes, I. L. Medintz, and W. R. Algar, "Quantum Dots as a Platform Nanomaterial for Biomedical Applications," in *Handbook of Nanobiomedical Research : Fundamentals, Applications and Recent Developments*

(Frontiers of Nanobiomedical Research), V. Torchilin, Ed. Singapore: World Scientific Publishing, 2014, pp. 621–662.

[6] J. A. H. Inkster, K. Liu, S. Ait-Mohand, P. Schaffer, B. Guérin, T. J. Ruth, and T. Storr, “Sulfonyl fluoride-based prosthetic compounds as potential ¹⁸F labelling agents.,” *Chemistry*, vol. 18, no. 35, pp. 11079–87, Aug. 2012.

PRESENTATIONS

[1] *Proteome Wide Unbiased Target Identification for Radiation Mitigating Drug Candidate using Thermal Proteome Profiling.*

Oral presentation at the American Society for Mass Spectrometry (ASMS) conference, Atlanta, GA. June 2019

[2] *Development of Protein Biomarkers for Radiation Injury Using Quantitative Mass Spectrometry.*

Oral presentation at ASMS conference, Indianapolis, IN. June 2017

[3] *Development of Protein Biomarkers for Effects of Radiation Exposure using Targeted Mass Spectrometry.* Lighting talk and poster presentation at US HUPO annual conference, San Diego, CA. Mar 2017

[4] *Time dependent development of organ-specific protein biosignatures in mouse plasma after radiation exposure.*

Poster presentation at the Radiation Research Society (RRS) annual meeting, Hawaii. Oct 2016

[5] *Development of Organ-Specific Protein Biomarkers for Effects of Radiation Exposure using Quantitative Mass Spectrometry.*

Poster presentation at ASMS conference, San Antonio, TX. June 2016

[6] *Development of plasma protein biomarkers for assessing radiation damage.*

Oral presentation at the inaugural session of “Brewin' Talks”, a UCLA biological sciences research showcase. May 2016

[7] *Optimizing MALDI-MS Based Virtual 2D Gel Method for Protein Characterization.*

Oral and poster presentation at the 14th Human Proteome Organization (HUPO) World Congress, Vancouver, BC. Sept 2015

CHAPTER 1: CURRENT STATUS ON MEDICAL PREPAREDNESS FOR UNEXPECTED RADIATION EXPOSURE

The threat of radiological and nuclear terrorism has been an increasing national security concern in recent years. Scenarios of concern include dispersion of radioactive materials, attacks on nuclear power plants, and the detonation of nuclear weapons.^[1] To address this concern, the National Institute for Allergy and Infectious Disease (NIAID) has established research programs to develop diagnostic tools to assess the levels of radiation injury and to develop countermeasure agents for use in the National Strategic Stockpile program.^[2] A key component of this initiative was the establishment of Centers for Medical Countermeasures against Radiation (CMCR), a network of academic institutions that drives the research programs. The UCLA CMCR is one of the 4 centers in the nation that is dedicated to radiation biodosimetry and drug development research.

An immediate consequence of ionizing radiation exposure is acute radiation syndrome (ARS). There are 3 types of ARS depending on the exposure dose: hematopoietic ARS (H-ARS), gastrointestinal ARS (GI-ARS), and cardiovascular/central nervous system ARS. H-ARS develops at moderate doses (2-6 Gy) because of the high radiosensitivity of progenitor cells. Neurovascular syndrome (>10 Gy) is generally considered untreatable due to multi-organ failure at such high levels of exposure.

Assessment of radiation injury in mass casualty scenarios is not trivial. Radiation victims might not initially show clear signs and symptoms of radiation toxicity even if exposed to substantial doses of radiation. In addition, there is considerable person-to-person variability in early and delayed radiation damage to organs and tissues in response to a given radiation dose due to factors such as genetic pre-disposition, age,

body size, underlying illnesses, and immune status. Therefore, estimates of radiation exposure dose alone (i.e. biodosimetry) will not necessarily predict the extent of radiation injury to organs and tissues. Traditional biodosimetry relies on detection of chromosome abnormality. However, in a mass casualty scenario, cytogenetic assays are not practical for diagnostic purposes because the process is time-consuming and requires experienced personnel for result interpretation.^[3] This assay is also limited to a whole-body dose estimate, and it can't properly assess heterogeneous exposure or severity of organ damage. Therefore, there is a need for development of radiation-specific biomarkers that can confirm exposure and predict acute and delayed radiation injury to specific organs and tissues to guide triage and treatment decisions.

The ideal radiation biomarkers should be measurable in a non-invasive or minimally invasive way, sensitive to incremental changes in radiation dose, and give a persistent signal (at least 24-hours post exposure). Proteins are highly desirable among all forms of molecular biomarkers because they can be accessible from body fluids, detectable with high-throughput methods such as mass spectrometry (MS), and most importantly, proteins are closely linked to physiological systems. To address the current lack of effective radiation biomarkers, we aim to develop and evaluate protein biomarkers that can assess organ-specific radiation damage using quantitative mass spectrometry techniques. Mass spectrometry has been used for biomarker discovery and validation over a decade due to its exquisite analytical specificity.^[4] In Chapter 2, a “shotgun” proteomics (discovery-based) experiment is used to identify biomarker candidates and pathways that are responsive to radiation. In Chapter 3, a targeted MS method is applied

to test a biomarker hypothesis based on a key radiation response pathway. This work is published in the *Journal of Proteomics – Clinical Applications*.^[5]

Medical treatment options for radiation victims are currently very limited. Despite decades of advances to develop radiation countermeasures for radiation injuries, few agents have been FDA approved for ARS.^[6,7] The type of countermeasures relevant to the context of unexpected radiation exposure is a radiomitigator, which is administered after radiation exposure in order to stimulate recovery of injured tissues. Currently available medical products have been developed only for treatment of hematopoietic ARS, and they are generally cytokines or growth factors such as granulocyte colony-stimulating factor (G-CSF) or granulocyte-macrophage colony-stimulating factor (GM-CSF).^[6,7] These drugs were originally developed for neutrophil stimulation in chemotherapy patients and were approved through drug repurposing for treatment of radiation victims. Part of the challenge with developing radiation countermeasures is that human clinical trials cannot be ethically conducted, and data from animal models have to be relied upon to predict human efficacy. To facilitate drug development efforts, the FDA passed the Animal Rule in 2002 that specified guidelines and requirements in order to use animal data for clinical indications. One of the four requirements is that the mechanism of injury and the role of the product towards the reduction of injury have to be understood.

The UCLA CMCR has a theme of discovery and development of novel drugs to mitigate acute and chronic radiation syndromes. Recently, CMCR researchers identified a group of compounds with a 4-nitrophenylsulfonamide backbone that showed efficacy for mitigating hematopoietic ARS.^[8] The compounds emerged from in vitro high-

throughput screening (HTS) for inhibitors of apoptosis. Some of these compounds were also tested for in vivo efficacy. The lead compound showed broad spectrum mitigation effects and anti-tumor action. The mechanism of action for the lead compound needs to be elucidated to advance the drug development process. In Chapter 4, a proteome-wide approach to target identification is described to discover a molecular mechanism for the lead molecule.

CHAPTER 2: DISCOVERY OF NEW ORGAN-SPECIFIC BIOMARKERS FOR RADIATION INJURY ASSESSMENT

2.1 Abstract

With increasing concern about nuclear/radiological terrorism, there is strong interest in developing a diagnostic platform to assess radiation injury following an incident. Traditional biodosimetry is insufficient for proper diagnosis and prognosis since victims may present delayed and/or varied response to radiation. There exists a critical need to develop more effective radiation injury biomarkers. To this end, we aim to develop protein biomarkers that can monitor organ-specific radiation response in the form of a blood test. In this study, we identified panels of candidate biomarkers from mouse bone marrow using label-free quantitative proteomics (LC-MS^E). C57Bl/6 male mice were sacrificed at various time points (2, 4, 8, 30 days) after whole body irradiation and their bone marrows were extracted for sample processing and analysis. Over 1800 proteins were identified and quantified from LC-MS^E data using Progenesis Q1 for proteomics data analysis. Proteins with differential expression after irradiation were classified based on their time course expression patterns. For proteins grouped into each temporal pattern, their biological functions and pathways were analyzed and compared. Finally, we devised the biomarker criteria for “durable” markers with persistent upregulation at later time points and for “stochastic” markers showing individual variation in radiation response. Based on the criteria, biomarker candidates for potential future investigations were proposed.

2.2 Introduction

The aim of this biomarker discovery project is to identify protein biomarkers in tissues and proximal fluids and then seek their presence and verify their expression levels in plasma towards the development of a diagnostic blood test for guiding treatment of radiation damage. Direct biomarker discovery in blood plasma or serum has not led to many successes in the past because of low abundant disease-related proteins in blood. Instead, approaches such as using proximal fluid and peripheral tissues can be favorable for initial selection of candidates.^[9] The tissue protein measurement in this study serves as a foundation for potential subsequent investigations of these signatures to be found in blood.

Following radiological or nuclear accidents, hundreds of thousands of people might potentially be exposed to radiation. Biodosimetry would help estimate the dose a person might have received, and whether the person needs acute care.^[10] Biodosimetry is critical for both triage and guiding the treatment of exposed population. Good biomarkers should robustly report radiation exposure, and preferably report the damage an individual sustained from radiation. Proteins, as part of cellular responses to radiation, are likely good indicators of biological damage.

In this experiment, bone marrow was selected as the target tissue for biomarker discovery because death in our mouse model following total body irradiation (TBI) is a result of lethal hematopoietic syndrome arising in bone marrow. Tissues were collected from control and irradiated mice sacrificed at various time points post 6 Gy TBI. We chose the sub-lethal dose of 6 Gy for these studies because it was desirable to avoid animals approaching death for our study (LD_{50/30} for C57 mice is 7.5 Gy).

2.3 Materials and Methods

Animals

C57Bl/6/JAX gnotobiotic male mice were bred and housed in the Radiation Oncology AAALAC-accredited animal facility at UCLA, and utilized at a body weight of 28gms (with 1S.D.<1gm; 9-12wks of age). Mice of both sexes in groups of four were matched to minimize variation in strain, age, weight and gender. Animal health was monitored at least daily and irradiated mice were followed more closely. Body weight was assessed twice per week. Euthanasia was by exposure to isoflurane and confirmed by cervical dislocation. There were no deaths due to irradiation or experimental procedures, as the dose and times were chosen to avoid hematologic ARS. The experiments were approved by the UCLA-IACUC and adhered to all federal and local regulations for the humane treatment of animals.

Irradiation

Total body irradiation (6 Gy) was performed using an AEC Gamma Cell 40 cesium irradiator (Cs-137) within the Animal Facility at a dose rate of around 60 cGy/min on unanesthetized mice in a well-ventilated Lucite box. Dosimetry was performed by the CMCR Physics Core at UCLA and involved the use of ionization chambers and chromographic film to assess beam flatness across the field (<5%). The LD50/30 dose for our C57Bl/6 mice is 7.5 Gy (50% animals survive after 30 days).

Bone Marrow Extraction

Bone marrow from the unirradiated control mice and irradiated mice after 2, 4, 8, and 30 days following 6 Gy TBI were extracted. The bone marrow was flushed from intact thigh bones of mice and cleaned with 70% ethanol using 5ml 1X PBS. The resulting bone

marrow suspension was centrifuged at 1,000 rpm in a clinical centrifuge and the pellet was frozen in a dry ice/ethanol bath and stored at -80°C.

Proteomic Sample Preparation

Bone marrow tissue was lysed in 900 µl lysis/reduction/alkylation all-in-one buffer containing 0.5% (w/v) sodium deoxycholate, 12 mM N-lauroylsarcosine, 10 mM tris(2-carboxyethyl)phosphine (TCEP), 40 mM chloroacetamide and 50 mM triethylammonium bicarbonate (TEAB). The samples were homogenized with a glass/PTFE Potter-Elvehjem tissue grinder using 5-6 hand strokes, followed by heating at 95°C for 5 minutes, and ultrasonication (Fisher Scientific Sonic Dismembrator Model 100) with 3 rounds of 10 sec bursts on ice. Samples were centrifuged at 16,000 g for 10 min and supernatants were collected. Protein concentration in the supernatant was measured using a Pierce BCA Protein Assay Kit (reducing agent compatible) following the manufacturer's protocols (Thermo Fisher), and a Shimadzu UVmini-1240 spectrophotometer. An aliquot of 50 µg total protein from each sample was diluted 5 fold with 50 mM TEAB. Trypsin (MS grade; Thermo Pierce) was added at a 1/100 enzyme to protein ratio and the sample was incubated at 37°C for 4 hours, followed by another 0.5 µg of trypsin addition and overnight incubation at 37°C. Digestion was quenched by addition of 0.5% trifluoroacetic acid. Detergent was removed by ethyl acetate extraction (equal volume to the sample) and the mixture was vortexed for 5 min. Samples were centrifuged at 16,000 g for 30 s and the top ethyl acetate layer was removed. Samples were dried down and resuspended in 100 µl Loading Buffer (3% acetonitrile/0.5% acetic acid). The C18/SCX StageTip was prepared for each sample by packing a layer of Empore™ Cation Extraction disk on the bottom and a layer of Empore™ C18 disk on the top in a 200 µl pipet tip. It was conditioned

by 100 μ l of 100% methanol, C18 Elution Buffer (80% acetonitrile/0.5% acetic acid), Loading Buffer (3% acetonitrile/0.5% acetic acid), SCX Elution Buffer (30% acetonitrile/500 mM ammonium acetate/0.5% acetic acid) and Loading Buffer, respectively. Each conditioning wash was followed by centrifugation at 2000 g for ~30 s. The peptide samples were loaded to the C18/SCX spin tips and centrifuged at 2000 g. They were washed with 100 μ l Loading Buffer, then with 100 μ l 3% acetonitrile/500 mM ammonium acetate/0.5% acetic acid, and finally with 100 μ l Loading Buffer each at 2000 g for ~30 s. Peptides that did not bind to the SCX filter were collected as the flowthrough with 20 μ l addition of C18 Elution Buffer. A 20- μ l step elution was performed with a syringe using the following dilutions of SCX Elution Buffer with varied ammonium acetate concentrations at: 17.5 mM, 20 mM, 35 mM, 50 mM, 65 mM, 80 mM, 100 mM, 300 mM, and 500 mM. These fractions, including the initial flow-through loading buffer wash, were dried down in a SpeedVac and then stored at -80°C until analysis.

Liquid Chromatography-Mass Spectrometry

Each fractionated sample was resuspended in 100 μ l injection buffer (3% acetonitrile, 0.5% acetic acid). For label-free quantification, Waters Hi3 *E.coli* ClpB standard (P63284, 6 synthetic peptide mixture) was spiked in to a 20 μ l sample aliquot to a final standard concentration of 10 fmol/ μ l. A pool sample was prepared from an equal aliquot from each time point (4 pool samples for each SCX fraction). All samples were analyzed in LC-MS^E mode on a Waters nanoAcquity UPLC system coupled to a Waters Xevo G2-XS mass spectrometer. The samples were grouped by SCX fraction, and different time points within the fraction were injected in randomized order. A total of 216 sample injections were performed (5 time points and 1 pooled sample \times 4 biological

replicates × 9 SCX fractions). The pooled sample was analyzed at the start and end of each block to ensure stability of the LC-MS/MS system.

A 5- μ l partial loop injection was injected into a Waters nanoAcquity UPLC M class system with a Symmetry C18 trap column (100 Å pore, 5 μ m particle, 180 μ m by 20 mm) and a HSS T3 analytical column (1.8 μ m, 75 μ m by 150 mm). Peptides were eluted with the following 90 min LC gradient: 7-27% B for the first 55 min, 27-45% B between 55-70 min, 45-85% B for the next 1 min, 85%B between 71-75 min, ramp down to 5% B for the next minute, and equilibrate at 5%B from 76 to 90 min (Solvent A is 0.1% formic acid in water, Solvent B is 0.1% formic acid in acetonitrile). Mass accuracy was maintained by a lock spray with a GluFiB internal standard peptide (m/z 785.8426). The mass spectrometer was operated in LC-MS^E sensitivity mode over the m/z 100-2000 range, with alternating energies from low CE of 6 V to a high CE between 18-45 V.

Data Processing

Raw MS data were imported into Progenesis QI for Proteomics v2.0 with the following parameters: lock mass m/z: 785.8426 Da, low energy threshold: 250 cts, elevated energy threshold: 100 cts, intensity threshold: 1000 cts, and retention time window: automatic. Each SCX fraction was analyzed separately in a single Progenesis experiment. Protein identification and quantitation results from all fractions were combined in the final analysis. Retention time for samples within each fraction (5 time points plus the pool × 4 biological replicates) were aligned automatically based on the most suitable reference pool. Peptide ions with charge state greater than 6 were excluded. To correct for systematic experimental variation across samples, normalization of peptide abundances to the spiked-in ClpB peptides was performed. Peptides were

identified by the MS^E search against the complete UniProtKB/Swiss-Prot *Mus musculus* database (accessed March 12, 2015, 85247 entries) with added common laboratory contaminants and from using the following parameters: trypsin as digest reagent, 500 kDa protein mass cutoff, maximum 2 missed cleavages, carbamidomethyl cysteine as a fixed modification, methionine oxidation as a variable modification, false discovery rate (FDR) of 4%, minimum 3 fragment ion matches per peptide, minimum 7 fragment ion matches per protein and minimum 1 peptide match per protein. Relative protein abundances were calculated from the average of the normalized abundances of three most abundant unique peptides (Hi-3 method). Absolute protein quantification was obtained based on 50 fmol Hi-3 ClpB calibrant protein (P63284) added. Protein measurements were exported for downstream statistical analysis.

2.4 Results and Discussion

2.4.1 The LC-MS^E label-free experiment

This LC-MS/MS-based discovery experiment captured time-dependent responses of proteins in bone marrow following exposure to ionizing radiation. In this study, C57BL/6 male mice were exposed to 6 Gy TBI. Unirradiated control mice (n=4) and irradiated mice after Day 2, 4, 8, and 30 (n=4 at each time point) were sacrificed, whereby their tissues were collected. The bone marrow samples were processed using a standard “shotgun” proteomics workflow consisting of tissue homogenization, lysis, protein denaturation, tryptic digestion and strong cation exchange (SCX) peptide fractionation prior to mass spectrometry analysis. A standard peptide mixture (Hi3 *E.coli* ClpB protein) was spiked into the sample as a calibrant for label-free quantitation. The digested peptide samples were analyzed by liquid chromatography with data-independent mass spectrometry using

a Quadrupole Time-of-flight (Q-TOF) instrument. In LC-MS^E mode, the instrument rapidly cycles between a low and high collision energy, so that both peptide precursor ions and their fragment ions are simultaneously collected.^[11,12] A software platform then matches the fragments to their precursors based on mass and LC retention time. This LC-MS^E label-free experiment achieves quantitation without expensive isotope labeling.

The mouse work was performed by Elizabeth Singer (UCLA). The mass spectrometry sample preparation and data acquisition were performed by a former postdoctoral fellow in our lab, Dr. Dyna Shirasaki. My contribution to this project started from the MS data processing and analysis.

Raw MS data were processed using Progenesis Q1 for Proteomics software. MS^E peptide ions were searched against the complete the Uniprot *Mus musculus* database to generate peptide and protein IDs. For protein quantitation, the average signals of the top 3 most intense unique tryptic peptides for each protein were used to represent the protein amount. The top 3 quantitation method has been adopted by the community as a label free proteomics workflow and it is based on the empirical discovery that the average MS signal response for the three most intense tryptic peptides per mole of protein is constant with a variation less than 10%.^[11] Relative protein concentration to the calibrant was computed for each run. With a known amount of Hi-3 ClpB calibrant that was spiked to every sample, absolute protein amount was determined. Finally, protein measurements were exported for downstream statistical analysis.

2.4.2 Global proteome changes after irradiation

A total of 1844 proteins from mouse bone marrow were identified and quantified from the combined LC-MS^E data from all SCX fractions using Progenesis analysis. The dynamic range of proteins quantified spans 8 order of magnitude.

By ranking proteins by their abundances, the most abundant ones are proteins involved in transcriptional regulation such as histone proteins and zinc finger proteins, as well as proteins that play key roles in the regulation of inflammatory process and immune response such as Protein S100-A9, a calcium- and zinc-binding protein (Figure 2.1).

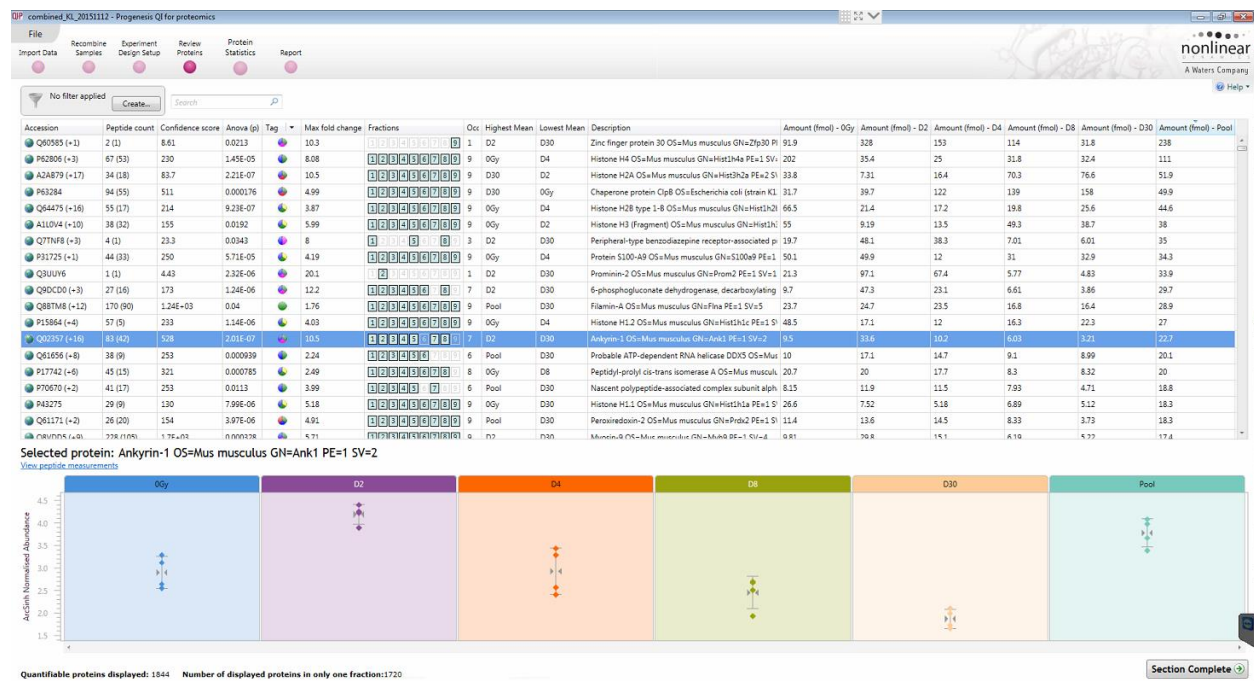


Figure 2.1: Proteins sorted by abundance of the pool (combined equal aliquot of 5 time points) in Progenesis Q1 for proteomics. Ankryin-1 protein was highlighted as an illustration, and its time course pattern was displayed at the bottom.

If proteins are sorted according to different time-course expression profiles, we observe early upregulation of DNA damage response proteins such as Protein PML and double-stranded DNA repair protein, which peaked at Day 4. We also observe proteins involved in DNA repair that peaked at Day 8 such as E3 ubiquitin-protein ligase SHPRH.

Lastly, we also see some late-stage DNA damage response factors such as Mediator of DNA damage checkpoint protein 1, which elevated at Day 30.

Recognizing the different time course profiles, we classified these proteins based on these four distinct patterns based on their abundances over time (Figure 2.2). Examples of proteins that display these patterns are shown in Figure 2.3. Based on these patterns, the general biomarker strategy we devised is the following: proteins within each pattern were subjected to pathway analysis and these pathways are investigated for their relevance in radiation response (Figure 2.4).

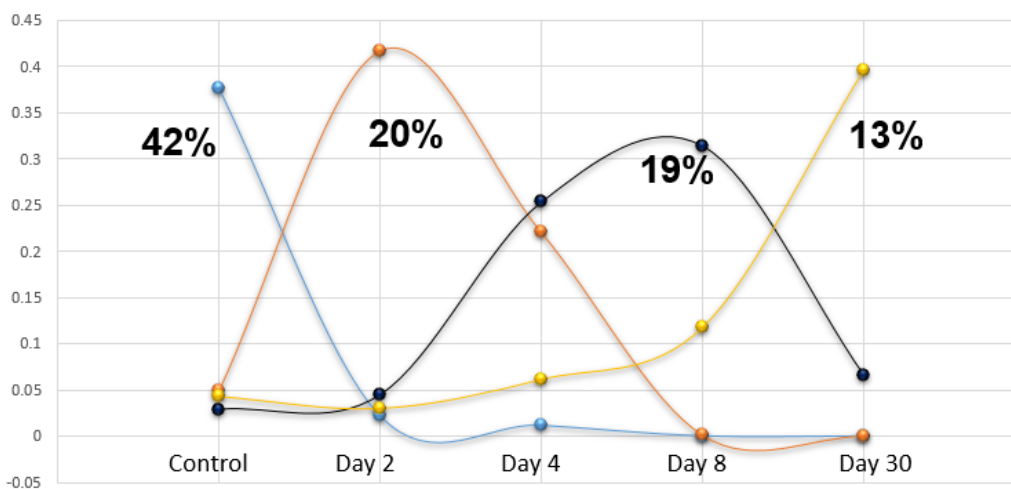


Figure 2.2: Differential time course expression patterns and the corresponding percentages of proteins that fell into each pattern. Light blue indicates proteins that decreased after radiation exposure and never recovered (42%); orange represents proteins that peaked at Day 2 (20%); dark blue represents proteins that peaked between Day 4-8 (19%); gold represents proteins that were elevated at Day 30 (13%).

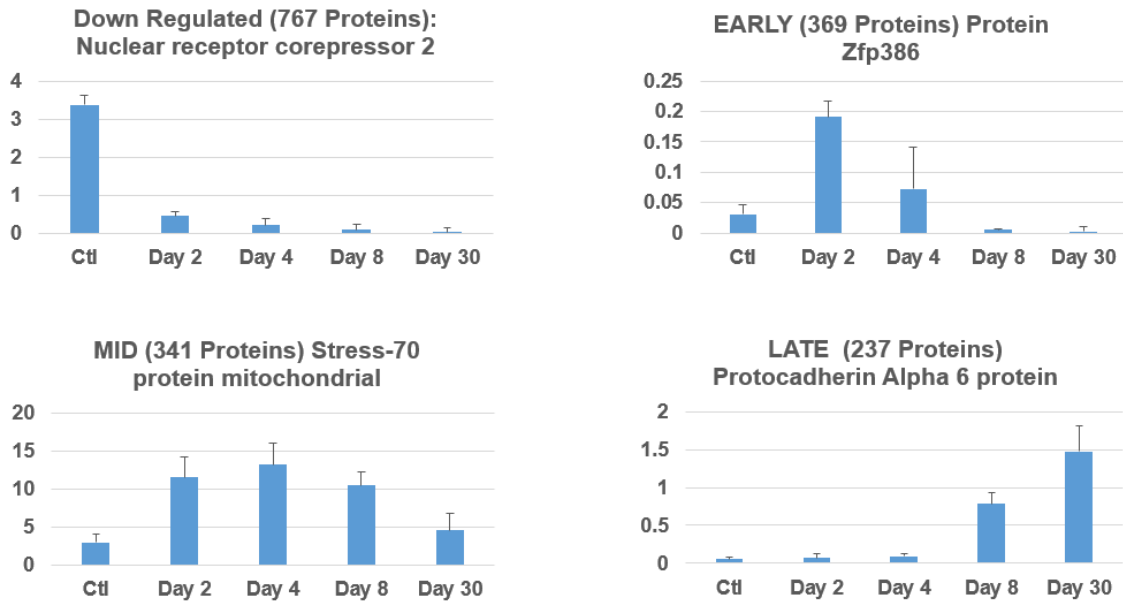


Figure 2.3: Protein examples of the 4 time course patterns.

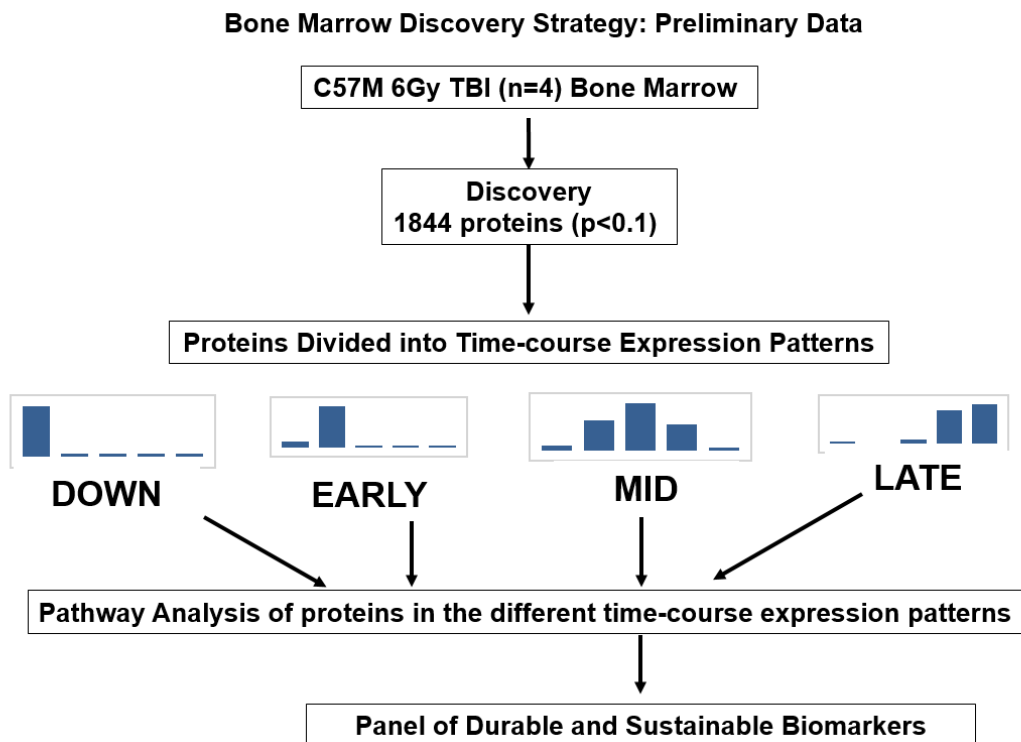


Figure 2.4: Biomarker discovery strategy based on time course patterns.

2.4.3 Pathway analysis of temporal protein expression patterns

Proteins were analyzed by PANTHER Gene Ontology (GO) protein classification and Ingenuity Pathway Analysis. From GO classification pie charts (Figure 2.5), we can see that the predominant biological processes were cellular processes, metabolic processes and cellular component organization. If we compare the proportions of these processes across the 4 time course patterns, we notice these differences and trends: (1) for early responders, there were more proteins classified as biological regulation and response to stimulus, which are the expected acute phase response after radiation exposure; (2) for mid-to-late phase activation, proteins involved in reproduction started to emerge, as cells were attempting to repair the damage after radiation; (3) for down-regulation, there was a greater portion of cellular component organization or biogenesis proteins, which is expected because many bone marrow cells undergo cell death or senescence after 6 Gy exposure. The same trends can also be visualized in the bar chart displaying the number of proteins that peaked at different time points for each biological process (Figure 2.6).

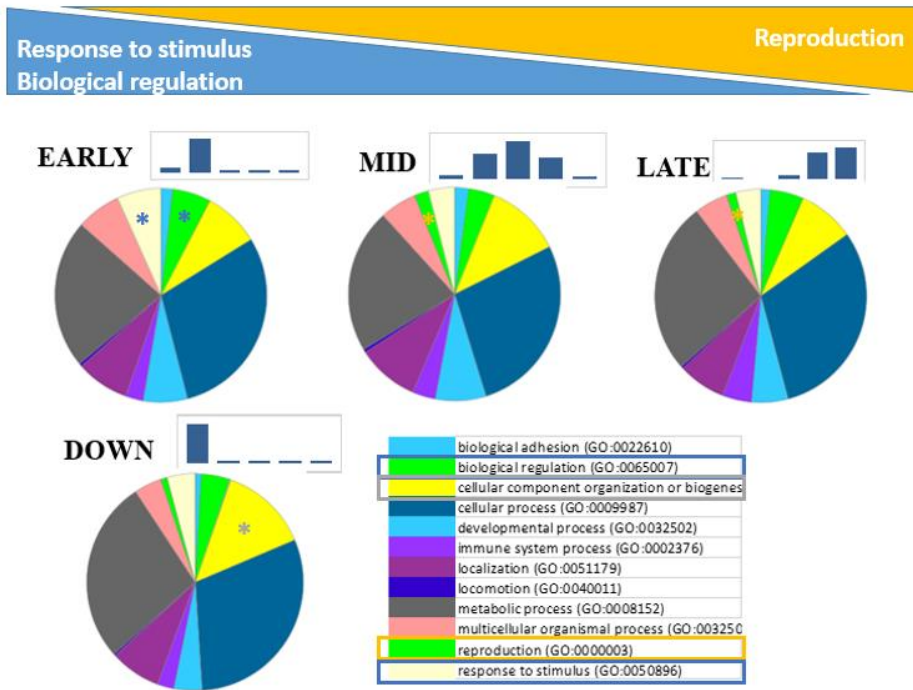


Figure 2.5: Pie chart of PANTHER GO-Slim Biological Process classification of proteins from each of the four time-course profiles. Asterisks highlights processes that differ in these 4 temporal profiles and they were color-matched to highlights in the legend.

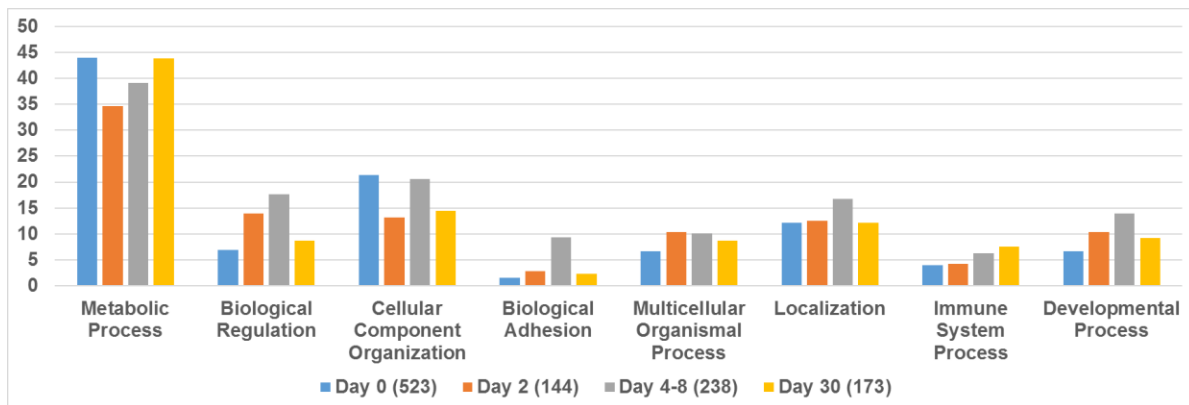


Figure 2.6: Bar chart of PANTHER GO-Slim Biological Process of bone marrow proteins at each of the four peak time points indicating number of proteins that fell into each category.

Wnt and Integrin signaling pathways are the key pro-survival radioprotective pathways. Interestingly in our pathway analysis, a significant number of proteins were mapped to these two signaling pathways (Table 2.1 and 2.2). Wnt signaling pathway is well-known for its involvement in tissue regeneration and repair after damage. In the context of radiation exposure, there have been many reports on involvement of Wnt

signaling in radioresistance and it was recently found that the radioresistance was mediated by high-mobility group box 1 protein (HMGB1), a chromatin-associated protein regulating DNA repair.^[13] Integrin-mediated adhesion to extracellular matrix proteins also offers resistance to radiation.^[14] Integrins in the cell membrane bind to extracellular matrix components and initiate actin reorganization and activation of MAPK and other signaling cascades. Pro-survival β 1A-integrin/Akt signaling mediated by PI3K was found to be critically involved in promoting cell survival after radiation injury.^[14]

Table 2.1: Proteins that were mapped to the Wnt pathway and their time course profiles and fold changes relative to unirradiated control mice.

WNT SIGNALING PATHWAY			
EARLY		Day 2/Ctl	
Transducin-like enhancer protein 2		1.99	
Adenomatous polyposis coli protein		1.80	
Inositol 1,4,5-trisphosphate receptor type 2		2.50	
Chromodomain-helicase-DNA-binding protein 1-like		7.53	
Protein Myh15		2.01	
Actin, alpha skeletal muscle		3.44	
Myosin-4		1.92	
Myosin-8		3.09	
Transcription factor 7-like 1		4.55	
Myosin-1		1.89	
MID		Day 4/Ctl	Day 8/Ctl
Inositol 1,4,5-trisphosphate receptor type 3		221.54	125.74
Myosin-6		1.91	0.60
Protocadherin-16		2.37	4.45
F-box/WD repeat-containing protein 1A		0.36	7.40
Myosin-7		1.98	0.75
Protein Myh15		2.15	1.47
LATE		Day 30/Ctl	
Protocadherin-19		9.11	
AT-rich interactive domain-containing protein 1A		1.60	
Protein Myh13		1.63	
F-box/WD repeat-containing protein 1A		16.28	
DOWN		Day 30/Ctl	
Actin, cytoplasmic 1		0.04	
Myosin-7B		0.32	
MCG140437, isoform CRA_d		0.66	
Follistatin-related protein 1		0.26	
Inositol 1,4,5-trisphosphate receptor type 1		0.17	
Phosphoinositide phospholipase C		0.46	
SWI/SNF-related matrix-associated actin-dependent regulator of chromatin subfamily A member 5		0.40	

Table 2.2: Proteins that were mapped to the Integrin pathway and their time course profiles and fold changes relative to unirradiated control mice.

INTEGRIN SIGNALLING PATHWAY		
EARLY		Day 2/Ctl
Phosphatidylinositol 4-phosphate 3-kinase C2 domain-containing subunit alpha		2.06
Alpha-actinin-4		1.89
Actin, alpha skeletal muscle		3.44
Laminin subunit alpha-2		3.34
MID		Day 4/Ctl
Alpha-actinin-1		2.36
LATE		Day 30/Ctl
Cell division control protein 42 homolog		2.35
Son of sevenless homolog 1		7.88
Laminin subunit beta-3		2.24
Collagen alpha-1(XII) chain		86.66
DOWN		Day 30/Ctl
Actin, cytoplasmic 1		0.04
Integrin-linked protein kinase		0.43
Beta-actin-like protein 2		0.40
Collagen alpha-1(III) chain		0.27
Vasodilator-stimulated phosphoprotein		0.46
Basement membrane-specific heparan sulfate proteoglycan core protein		0.24
Integrin beta-7		0.33
Protein Col4a6		0.46
Actin-related protein 2/3 complex subunit 5		0.37
Laminin subunit gamma-1		0.00
Alpha-actinin-3		0.57
Collagen type V alpha 3 chain		0.03
Collagen alpha-2(I) chain		0.34
Actin-related protein 2/3 complex subunit 1B		0.46
DOWN WITH RECOVERY		Day 30/Ctl
Ras-related C3 botulinum toxin substrate 2		0.52
Integrin alpha-11b		0.32

2.4.4 Bone marrow as a sentinel organ

For the physiological changes in the mouse as a whole, 6Gy total body irradiation induces double-stranded DNA breaks and damage in multiple organs. After TBI, proteins in the bone marrow respond to the damage directly in the bone marrow as well as respond to signals from the outside (Figure 2.7). Signals from damaged tissues such as lung and gut can leak into bloodstream. Cytokines are released into the bloodstream by damaged tissues within minutes to hours. These cytokines travel to the bone marrow and enter the stem cell niche, which then induces stem cell differentiation and evacuation out of bone marrow.

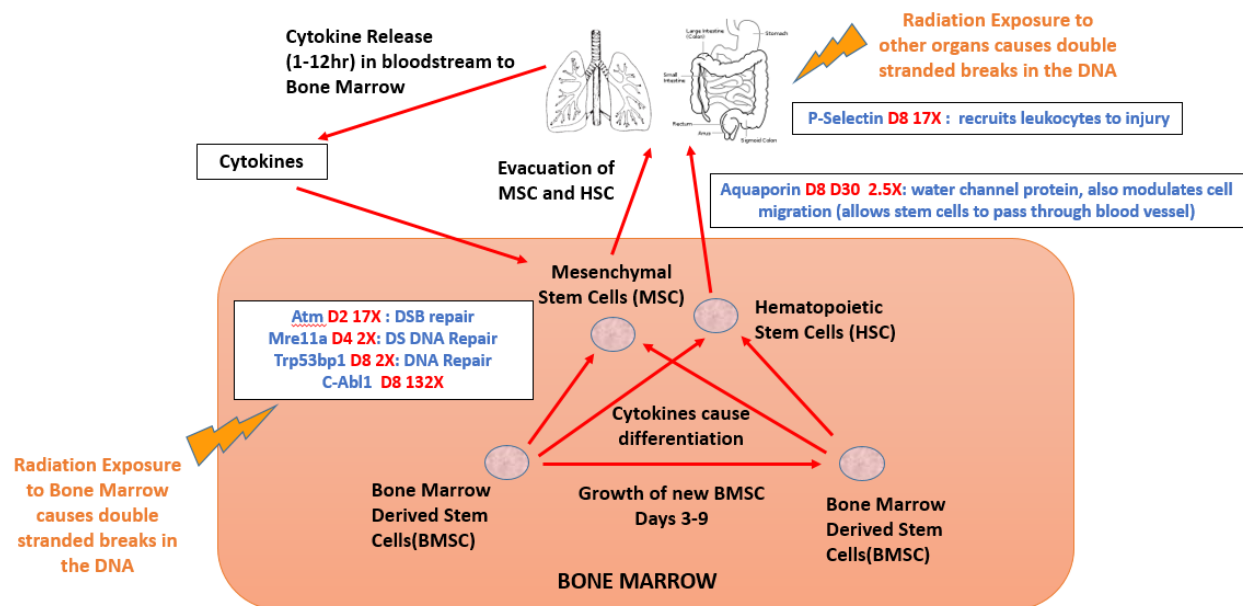






Figure 2.7: Bone marrow responds to damage from inside and outside.

2.4.5 Proteins with biodosimetry potential

We established the following criteria for durable and sustainable biomarker candidates: greater than 2 fold elevation on Days 4 and 8 ($p < 0.05$). Day 4 and Day 8 were selected for two main reasons: bone marrow response within this time window seems to be critical to the final survival and recovery of the mice after TBI; these are more realistic time points when blood from radiation victims will be screened for diagnosis in a mass casualty scenario. Of the 1844 proteins quantified, 156 proteins were found to be elevated at least 2 fold at Days 4 and 8. These identified proteins were found to be involved in different cellular responses and metabolic processes with functional attributes like DNA synthesis, protein synthesis and degradation, apoptosis, oxidative stress. Examples of durable biomarker candidates from the Integrin and Wnt signaling pathways are shown in Table 2.3.

Table 2.3: Examples of durable biomarker proteins in the Integrin and Wnt signaling pathways.

Proteins	Day 4/Ctl	Day 8/Ctl	Time Course	Pathways
Son of sevenless homolog 1	2.14	7.88		Integrin Signalling
Collagen alpha-1(XII) chain	14.63	86.66		Integrin Signalling
Inositol 1,4,5-trisphosphate receptor type 3	221.54	125.74		WNT Signalling
Protocadherin-16	2.37	4.45		WNT Signalling

At Day 8, prominent physiological changes in mice were observed: the bone marrow appeared pale and thin, the spleen became smaller and fur whitening was also observed. Day 8 seems to be a critical transition point in radiation response because we observed significant individual variation among the biological replicates. These protein abundances at Day 8 might correlate to the stochastic response in mouse survival. A simplistic explanation of the differential survival is that in some individuals most hematopoietic stem cells are destroyed while in others there are sufficient remaining viable stem cells for animal survival beyond 30-days with an apparent recovery from the insult.

Finally, among proteins that fulfilled our general biomarker criteria, we collected a panel of proteins with robust up-regulation at 8 days post-TBI, which represents ‘durable’ markers of radiation exposure that might predict a stochastic response (Table 2.4). This set of proteins is worth further investigation for use in dosimetry.

Table 2.4: Biomarker panel for that may be predictive for a stochastic response (greater than 2 fold up-regulation at Day 8).

Protein	ID	Peptides Total/Unique	Intensity Day 8/0	Ratio Day 8/0	Function	Role in Disease	Pathways	Peptides for PRIM
Arachidonate 15-lipoxygenase	P39654	9/4	0.257/0.016	16.1470016	Enzyme in the metabolism of polyunsaturated fatty acids	inhibit, limit, and resolve diverse inflammatory diseases	Inflammation mediated by chemokine and cytokine signaling pathway, Gonadotropin releasing hormone receptor pathway	DGTILNVAATSISDLPVDQR SLDIPYEYLRPSLVNSVAI GPGDQGGSEYTFPCYR
Alpha-actinin-1	Q7TPR4;A1BNS4;D3YY95;Q61063;Q99LJ3	69/19	13.6/5.75 (Day 4)	2.36			Integrin Signaling	DYETATLSEIK LLETIDQLYLEYAKR FAIQDISVEETSAAKGLLLWCQR
Son of sevenless homolog 1	Q62245	4/2	1.119/0.475	7.88	Promotes the exchange of Ras-bound GDP by GTP.		Integrin Signaling, EGFR, FGF, Inflammation mediated by chemokine and cytokine signaling pathway, Angiogenesis, CCKR Signaling, Gonadotropin releasing hormone receptor pathway	LDHTEFQIPSR QAQQLPYEFFSEENAPK
Cell division control protein 42 homolog	P60766;Q3UL78	5/3	1.119/.475	2.35	Activated Cdc42 phosphorylates p21-activated kinases PAK1 and PAK2, which in turn initiate actin reorganization and regulate cell adhesion, migration, and invasion.	promoting the expression of β 1 integrin which is important for adhesion to the extracellular matrix	Inflammation mediated by chemokine and cytokine signaling pathway; Integrin Signaling	NVFDEAILAALPEPEPK YVECSALTQK
Collagen alpha-1(XII) chain	Q60847;E9PX70;Q3TNZ7;	3/1	0.391/0.00452	86.66	Enzyme in the metabolism of polyunsaturated fatty acids		Inflammation mediated by chemokine and cytokine signaling pathway	NSDVEIFAVGVKDAVR
Laminin subunit alpha-2	Q60675;Q5DTP0	13/3	1.72/.822	2.09	Enzyme in the metabolism of polyunsaturated fatty acids		Integrin Signaling	IYFGGLPTLRNLSMK
Inositol 1,4,5-trisphosphate receptor type 3	P70227	4/1	0.254/0.002	125.7	Enzyme in the metabolism of polyunsaturated fatty acids	inhibit, limit, and resolve diverse inflammatory diseases	Inflammation mediated by chemokine and cytokine signaling pathway, Heterotrimeric G-protein signaling pathway-Gq alpha and Go alpha mediated pathway, Histamine H1 receptor mediated signaling pathway, Endothelin signaling pathway, Gonadotropin releasing hormone receptor pathway, Wnt Signaling Pathway	FSGMKCSECSR IYFGGLPTLRNLSMK TAVADNLLFLYLSAK
LIM/homeobox protein Lhx2	P39654	9/4	0.257/0.016	16.1470016			Gonadotropin releasing hormone receptor pathway	SYFAINHNPDAK
Nitric oxide synthase, brain	Q9Z0J4;F8WGF2;Q9Z0J4-2;Q9Z0J4-5;S4R255	3/2	0.342/0.0441	7.76			Gonadotropin releasing hormone receptor pathway, CCKR Signaling	GMNPPMVLVFGCRQSK SSGDGPLDRDNFESTGPLANVR
Ephrin type-A receptor 3	P29319	2/1	11.426/2.886	3.95			Angiogenesis	CGWNVVRQCEPCSPNVR
Glycogen phosphorylase, brain	Q8C194;Q3TFQ8;Q3UGT5;Q3UYH9;Q3UZL2;Q3V3U0	24/6	1.703/0.85	2.002			Heterotrimeric G-protein signaling pathway-Gi alpha and Gs alpha mediated pathway	QAVDQISSGFFSPK GYNAREFYER
Regulator of G-protein signaling 3	Q9DC04;Q9DC04-1	2/1	0.1844/0.072	2.53			Heterotrimeric G-protein signaling pathway-Gi alpha and Gs alpha mediated pathway, Heterotrimeric G-protein signaling pathway-Gq alpha and Go alpha mediated pathway	HSCHLVCDDSSDGLLGGWER
Regulator of G-protein signaling 7	O54829	1/1	0.213/0.023	9.16			Heterotrimeric G-protein signaling pathway-Gi alpha and Gs alpha mediated pathway	AFWDVHRPVGCVNTEVDIKK
Platelet-derived growth factor D	Q92517	1/1	3.404/1.0057	3.385			Angiogenesis	LTNAVFFPR

2.5 Conclusion

Protein markers proposed from bone marrow can be further tested in plasma using protein depletion or enrichment strategies prior to mass spectrometry detection. Similar biomarker discovery approaches can be applied to other organs like lung or gut to screen for organ-specific markers. The overarching goal of this project is to readout an individual's radiation dosimetry and to predict stochastic, organ-specific responses with a rapid blood test taken days after radiation exposure.

CHAPTER 3: EVALUATION OF BIOMARKER POTENTIAL OF NRF2-MODULATED ANTIOXIDANT RESPONSE PROTEINS

3.1 Abstract

Potential acute exposure to ionizing radiation in nuclear or radiological accidents presents complex mass casualty scenarios that demand prompt triage and treatment decisions. Due to delayed symptoms and varied response of radiation victims, there is an urgent need to develop robust biomarkers to assess the extent of injuries in individuals. The transcription factor Nrf2 is the master of redox homeostasis, as it regulates the basal and inducible expression of antioxidant and detoxification genes. Based on prior transcriptional evidence of Nrf2-dependent antioxidant response activation upon radiation, we investigated the biomarker potential of Nrf2-dependent downstream target enzymes by measuring their response in bone marrow extracted from C57Bl/6 and C3H mice of both genders for up to 4 days following 6 Gy total body irradiation using targeted mass spectrometry. Overall, C57Bl/6 mice have a stronger proteomic response than C3H mice. In both strains, male mice have more occurrences of upregulation in antioxidant enzymes than female mice. For the more frequently studied C57Bl/6 male mice, 3 proteins showed elevated abundances after radiation exposure ($p < 0.01$): catalase, superoxide dismutase 1, and heme oxygenase 1. Across both strains and genders, glutathione S-transferase Mu 1 was consistently decreased, making it the most promising biomarker candidate from our study.

3.2 Introduction

Despite continual risk of radiation from nuclear accidents and terrorist attacks, effective assessment of acute radiation exposure remains to be established for triage and treatment of the population.^[10,15] Following a radiological event, several stages of mass screening utilizing a combination of physical and biological dosimetry methods will be needed to establish the severity of any radiation exposure. Traditionally, clinical determination of radiation dose relies on cytogenetic assays such as chromosome aberration, which normally involves lymphocyte cell culture and scoring of abnormalities. This process is time consuming and requires experienced personnel, making it unsuitable for triage of a mass-casualty event.^[3,10,15] In addition, cytogenetic assays from blood yields a crude total body dose estimate, which is not ideal given that accidental exposure is likely heterogeneous and there is considerable difference in organ sensitivities to radiation. On the other hand, protein biomarkers can offer molecular insights into the physiology of cells and tissues that can guide organ-specific medical treatment. Despite the advantages of proteomics, it has been underutilized in radiation research historically, which leads to a scarcity in radiation proteomics knowledge^[16] and a shortage of well-established tissue-specific biomarkers.^[17]

Some of the special challenges for proteomic analysis of radiation biology are due to subtle alterations in cell or tissue proteome, even after high dose exposure.^[18] This impacts the majority of radiation proteomics studies and as a result there has been suggestions to apply a fold change cutoff lower than 1.5 for biological significance in radiation research.^[18] In recent years, applications of proteomics in radiation research have increased with advancement in high throughput mass spectrometry technologies.

Several groups have developed or implemented state-of-the-art quantitative proteomics tools to identify and validate protein biomarker signatures associated with radiation exposure.^[19–23] Our focus has been on the master regulator of anti-oxidant responses, NF-E2-Related Factor 2 (Nrf2).

Ionizing radiation (IR) causes a multitude of effects on cells. Radiation can directly damage DNA and other biomolecules or indirectly through generation of free radicals and reactive oxygen species (ROS) leading to acute radiation syndromes (ARS) and chronic effects of radiation including carcinogenesis, fibrosis, inflammation, and genomic instability.^[24,25] In an attempt to maintain redox homeostasis, cellular antioxidant defense mechanisms that are composed of small molecular antioxidants and antioxidant enzymes are activated. Many antioxidant enzymes are regulated by a key transcription factor, Nrf2. Nrf2 is normally sequestered by Keap1 protein in the cytoplasm. Upon activation by signals such as ROS, the Nrf2-Keap1 complex is disrupted, leading to nuclear translocation of Nrf2 and binding to the Antioxidant Response Element (ARE), which in turn regulates expression of downstream antioxidant and detoxification genes that boost cell survival.^[26] These target genes include glutathione S-transferase (GST), UDP-glucuronosyltransferases, γ -glutamylcysteine synthetase (γ -GCS), glutathione peroxidase, superoxide dismutase 1 (SOD1), heme oxygenase 1 (HO-1), catalase, and NADPH: quinone oxidoreductase (NQO-1). These enzymes have been repeatedly demonstrated to be cytoprotective against insult, and Nrf2 is assumed to be a key regulator for inducible expression of these enzymes.^[27,28]

Two articles published in 2010 reported Nrf2 transcriptional activation following ionizing radiation. Tsukimoto *et al.* showed that low dose gamma rays induced Nrf2

activation in mouse macrophage RAW264.7 cells.^[29] A separate study by McDonald *et al.* also observed similar Nrf2 induction in different systems.^[30] They found that single doses of ionizing radiation from 2 to 8 Gy activated ARE-dependent transcription in breast cancer cells in a dose-dependent manner. They also observed increased radiosensitivity in Nrf2 knock out cells and mice after irradiation.^[30] More interestingly, a recent transcriptional study by Purbey *et al.* identified ROS activation of Nrf2 as an important IR sensing pathway.^[31] Their study reveals that Nrf2 activation by ROS is highly selective to radiation exposure as opposed to other environmental insults. In their RNA-Seq data from C57Bl/6 bone marrow derived macrophage (BMDM) collected 0.5-24 hr after 6 Gy irradiation, only 99 genes (1.1%) were induced more than 4-fold, which is in accordance with the common observation of subtle changes in the proteome upon irradiation. Among these few potentially induced genes, Nrf2-regulated gene expression peaked between 1-2 hr and were classified as early response genes.

Besides potent induction of Nrf2 after IR, studies also indicated different induction kinetics in different cell types.^[32] For example, in the two initial reports, Tsukimoto *et al.* observed a rapid induction in mouse RAW264.7 macrophage cells, whereas McDonald *et al.* found a delayed response of 5 days in other cell types. The different induction kinetics can be useful to differentiate the origin of damage. Another factor that can be utilized to localize Nrf2 response is isoform-specific tissue distributions. For instance, GST enzyme is highly polymorphic and it consists of 25 isoforms in mice and also in human (taken from Uniprot). A study mapping out GST tissue distributions in mouse reported differential expression of these isoforms in different tissues, and some isoforms were predominantly expressed in certain tissues.^[33]

Therefore, based on the existing evidence of robust and dose-dependent induction of Nrf2 following IR and other desirable features such as differential induction kinetics and tissue-specific expression, we hypothesized a biomarker potential for Nrf2-mediated response proteins in assessment of ionizing radiation exposure and related organ damage. Potentially, these proteins can be used towards development of a diagnostic blood test for exposure and feedback of efficacy of mitigatory treatment in radiation emergencies.

In this study, using a targeted proteomics approach with mass spectrometry (MS), we examined the response of Nrf2-ARE-dependent enzymes in mouse bone marrow collected at various time points (8 hours to 4 days) after 6 Gy total body irradiation (TBI) in two mouse strains and both genders. The strain and gender groups offer a representation of varied radiation response in a population due to different genetic backgrounds. Bone marrow is investigated in this initial study because it is a highly radiosensitive organ and the responses of the hematopoietic system are major determinants of outcome after IR exposure.^[34] A high sublethal dose of 6 Gy TBI causes significant damage to bone marrow and hematopoietic acute radiation syndrome (H-ARS) in mice. Nrf2-mediated response is particularly important in this context because Nrf2 activation is also known to enhance hematopoietic stem progenitor cell function and mitigate IR-induced bone marrow suppression and mortality.^[35,36] The measurement of Nrf2-ARE-dependent proteins in bone marrow in this study may provide insights to hematopoietic recovery of mice and this study serves as a foundation to potential subsequent investigations of these signatures in blood. Direct biomarker discovery in blood plasma or serum has not led to many successes in the past because of low

abundant disease-related proteins in blood. Instead, approaches such as using proximal fluid and peripheral tissues can be favorable for initial selection of candidates.^[9]

3.3 Materials and Methods

Animals

C3Hf/Sed//Kam and C57Bl/6/JAX gnotobiotic male and female mice were bred and housed in the Radiation Oncology AAALAC-accredited animal facility at UCLA, and utilized at a body weight of 28gms (with 1S.D.<1gm; 9-12wks of age). Mice of both sexes in groups of eight were matched to minimize variation in strain, age, weight and gender. Animal health was monitored at least daily and irradiated mice were followed more closely. Body weight was assessed twice per week. Euthanasia was by exposure to isoflurane and confirmed by cervical dislocation. There were no deaths due to irradiation or experimental procedures as the dose and times were chosen to avoid hematologic ARS. The experiments were approved by the UCLA-IACUC and adhered to all federal and local regulations for the humane treatment of animals.

Irradiation

Total body irradiation was performed using an AEC Gamma Cell 40 cesium irradiator (Cs-137) within the Animal Facility at a dose rate of around 60 cGy/min on unanesthetized mice in a well-ventilated Lucite box. Dosimetry was performed by the CMCR Physics Core at UCLA and involved the use of ionization chambers and chromographic film to assess beam flatness across the field (<5%). The LD70/30 dose for our C3H/Sed mice is 7.73 Gy. For C57Bl/6 mice, it is 8.51 Gy.

Bone Marrow Extraction

At 8 hour, 1, 2 and 4 days after TBI, bone marrow was extracted. The bone marrow was flushed from intact thigh bones of mice and cleaned with 70% ethanol using 5ml 1X PBS. The resulting bone marrow suspension was centrifuged at 1,000 rpm in a clinical centrifuge and the pellet was frozen in a dry ice/ethanol bath and stored at -80°C.

Proteomic Sample Preparation

Bone marrow tissue was lysed in 0.5% (w/v) sodium deoxycholate, 12 mM N-lauroylsarcosine, and 50 mM triethylammonium bicarbonate (TEAB). The samples were homogenized with a bead beater (Bullet Blender; Next Advance, Inc.) at max. speed for 1 min, followed by heating at 95°C for 5 minutes, and sonication in a water bath for 5 min. Samples were centrifuged at 16,000 g for 5 min and supernatants were collected. Protein concentration in the supernatant was measured using a Pierce BCA Protein Assay Kit following the manufacturer's protocols (Thermo Fisher). An aliquot of 50 µg total protein from each sample was reduced with 5 mM tris(2-carboxyethyl)phosphine for 30 min at room temperature and alkylated with 10 mM iodoacetamide in the dark for 30 min at room temperature. The protein samples were then diluted 5 fold with 50 mM TEAB. Trypsin (MS grade; Thermo Pierce) was added at 1/100 enzyme to protein ratio and the sample was incubated at 37°C for 3-4 hours, followed by another 0.5 µg of trypsin addition and overnight incubation at 37°C. Digestion was quenched by 0.5% trifluoroacetic acid. Samples were centrifuged at 16,000 g for 5 min and supernatants were collected and dried under vacuum. Samples were desalted with C18 Stagetips made from Empore C18 solid phase extraction disks. The desalted samples were stored at -80°C until use.

Surrogate Peptide Selection

Proteotypic peptides for Nrf2-modulated proteins were selected from PeptideAtlas (www.peptideatlas.org) with preference for high empirical suitability score, number of observations and proteotypic score. Peptides were filtered according to the following criteria: 8-25 amino acid in length, no missed cleavage site, and no possible modification sites such as cysteine, methionine, tryptophan, and N-terminal glutamine. Candidate peptides were further evaluated by their performance in Parallel Reaction Monitoring (PRM) experiments using a control bone marrow sample. The top 2 peptides were selected as surrogates for each protein for the PRM assay (Table 3.1). Peptide uniqueness was confirmed by searching against the NCBI Protein Reference Sequence database for *Mus musculus* using BLASTp (exceptions: peptide ITQSNAILR belongs to multiple isoforms of GST proteins and peptide YTGTRPSNLAK belongs to multiple isoforms of UGT).

Table 3.1: Protein and surrogate peptides. Peptides with asterisks are not unique to the protein isoform. Bolded peptides are the final 6 surrogate peptides used in quantitation.

Protein Name	Gene (Protein Abbrev.)	Peptide	Mass [m/z]
catalase	CAT	FNSANEDNVTQV(R)	747.35
		NFTDVHDPYGA(R)	464.55
glutathione peroxidase 1	GPX1	YVRPGGGFEPNFTLFE(K)	653.33
		AHPLFTFL(R)	367.88
glutamate-cysteine ligase regulatory subunit	GCLM (GSH0)	LFIVGSNSSST(R)	677.85
		IVAIGTSDL(D)(K)	566.32
glutamate-cysteine ligase catalytic subunit	GCLC (GSH1)	SLFFPDEAIN(K)	640.83
		VVINVPF(K)	514.83
glutathione S-transferase Mu1	GSTM1	ITQSNAIL(R) *	508.30
		YIATPIFS(K)	520.29
heme oxygenase 1	HMOX1 (HO-1)	THPELLVAHAYT(R)	754.40
		YLGDLGGQVL(K)	625.34
NADPH dehydrogenase [quinone] 1	NADPH1 (NQO1)	NFQYPSSESLAY(K)	767.36
		FGLSVGHHLG(K)	576.32
superoxide dismutase [Cu-Zn]	SOD1	GDGPVQGTIHFEQ(K)	756.88
		HVGD LGNV TAG(K)	584.31
UDP-glucuronosyltransferase 1-1	UGT 1-1	GHEVVVIAPEASIH(I)(K)	566.99
		YTGTRPSNLA(K) *	604.33

Crude stable isotope-labeled standard (SIS) peptides (^{13}C , ^{15}N on C-terminal R/K) for the 18 peptides in Table 3.1 were synthesized by Thermo Pierce. The heavy peptides were diluted with injection buffer (3% acetonitrile, 0.1% formic acid) and pooled to make a final concentration of either 10 nM or 100 nM in the SIS mixture to match the concentrations of endogenous peptides in the sample.

Liquid Chromatography-Mass Spectrometry

Each sample was resuspended in 100 μl injection buffer. An equal volume of SIS mixture was added to the sample for relative quantitation. All samples were subjected to analysis on an Easy-nLC 1000 system coupled to a Q-Exactive mass spectrometer (Thermo Fisher Scientific). The samples were grouped into injection blocks that covered all conditions of comparison (time points, strains, genders). Each block containing 20 samples was injected in a randomized order and analyzed in targeted-MS² mode with retention time scheduling (4 min window). Triplicate injections of 8 biological replicates were analyzed over 480 runs. An *E.coli* digest standard (1 $\mu\text{g}/\mu\text{l}$) was analyzed at the start and end of each block to ensure stability of the LC-MS/MS system.

A 4- μl injection was loaded onto a 75 μm i.d. \times 25 cm EASY-Spray analytical column (Thermo Fisher Scientific). Peptides were eluted in a 50 min gradient of mobile phase A (0.1% formic acid in water) and mobile phase B (0.1% formic acid in acetonitrile) at a flowrate of 300 nl/min: 5% B at 0 min, 29% B at 32 min, and 80% B from 40.5-50 min. The spray voltage was 2 kV and the capillary temperature was 250 $^{\circ}\text{C}$. The mass spectrometer was operated in a targeted-MS² acquisition mode with a maximum IT of 130 ms, 1 microscan, 35 000 resolution, 2E5 AGC target, 1.6 m/z isolation window, and 27% normalized collision energy.

PRM Assay Quantitative Performance

While 18 peptides were monitored in the assay, the 6 most reliable peptides representing 6 proteins were used for final quantitation and these peptides were indicated in Table 3.1. Linearity of PRM response for these peptides was evaluated by spiking varying amounts of heavy standard peptides into a constant matrix made from pooling C57Bl/6 male control mouse bone marrow digest samples, based on the “reverse curve” method described in Percy, *et al.*^[37–40] The final heavy peptide concentrations in the pool were either 0.05, 0.5, 5, 50, 500 nM or 0.5, 5, 50, 500, 5000 nM depending on the peptide (the range was adjusted to match concentrations of endogenous peptides). Triplicate injections were performed to construct the reverse response curve. The linear range spanned more than four orders of magnitude, and our measurements lay within the linear range of the assay (Supplementary Figure S3.1).

The extent of carryover was also tested by running replicate injections of 4 randomly chosen samples in different injection orders and compared the peak area ratios of target peptides. No significant differences in the peak area ratios between replicates were observed, suggesting sample carryover in our LC-MS system was minimal. There was also no detectable target peptide in blank runs following sample runs in PRM mode.

Stable Isotope Label-based Relative Quantification

Raw PRM data were processed in Skyline (version 3.6.0, MacCoss lab, University of Washington). Public MS/MS spectral libraries for *Mus musculus* were uploaded to Skyline from National Institute of Standards and Technology and Global Proteome Machine databases. The Uniprot FASTA file for *Mus musculus* (82124 protein entries) was added to Skyline as the background proteome. Extracted chromatograms for target

peptides were manually inspected to ensure correct peak detection. Better performing peptides with the top three to five transitions were selected for quantification based on the higher dot product correlation between the observed transitions of target peptides and library spectrum, indicating higher confidence in peptide detection. Summed peak area ratios of endogenous versus SIS peptide transitions were obtained for the preliminary relative quantification result.

Statistical Analysis using MSstats

Statistical analysis was performed with the MSstats package (version 3.6.0) implemented in R. Data were divided into 4 groups: C57 male, C57 female, C3H male, C3H female. Within MSstats, peak intensities were first log₂ transformed, and normalized to equalize medians in log₂ intensities in all runs within a group of comparison. The intensities of the features of a protein in a run were summarized to obtain a single value per protein per run, using Tukey's median polish (accounted for missing values). Finally, to test protein abundances for significant changes of each time point compared to unirradiated control, a linear mixed effect model was applied and adjusted p-values (accounting for multiple comparisons) were obtained.

3.4 Results and Discussion

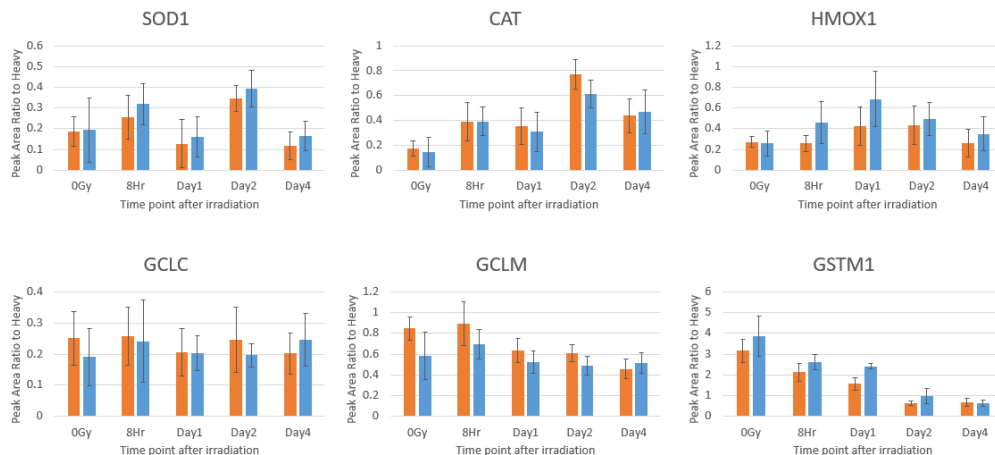
3.4.1 PRM assay development and relative quantification result in Skyline

Statistical design of mass spectrometry experiments was taken into consideration in our assay development.^[41] Samples were grouped into randomized injection blocks to minimize instrument bias and batch-to-batch variation over month-long data acquisition. Within each block, there were 20 samples covering all conditions of comparison, including 4 mouse groups (two strains and genders) and 5 time points. Samples were analyzed in

random order within each block. Eight blocks of biological replicates were cycled three times to obtain triplicate measurements.

With respect to peptide performance in the PRM assay, six out of the nine putative protein targets were reliably detected in the biological samples. The remaining three proteins had run-to-run inconsistencies either in standard or endogenous peptide levels. The Glutathione Peroxidase 1 standard peptides had too much variation in intensity between different sample preparations, possibly caused by hydrophobicity issues that resulted in variable peptide loss. NAD(P)H dehydrogenase [quinone] 1 and UDP-glucuronosyltransferase 1-1 endogenous peptides were not reliably detected, possibly due to low abundance in this complex matrix. It is conceivable that other more detectable peptides exist for these proteins if we relax the peptide selection criteria, but in doing quantification accuracy may be compromised. For the final analysis, only one best-performing peptide per target protein was included and their top 3-5 transitions based on dot product and reproducibility were used in quantitation. Summed peak area ratios of endogenous versus SIS peptide transitions in Skyline were obtained for visualization of the raw relative quantification result (Figure 3.1).

(a) C57Bl/6 mice



(b) C3H mice

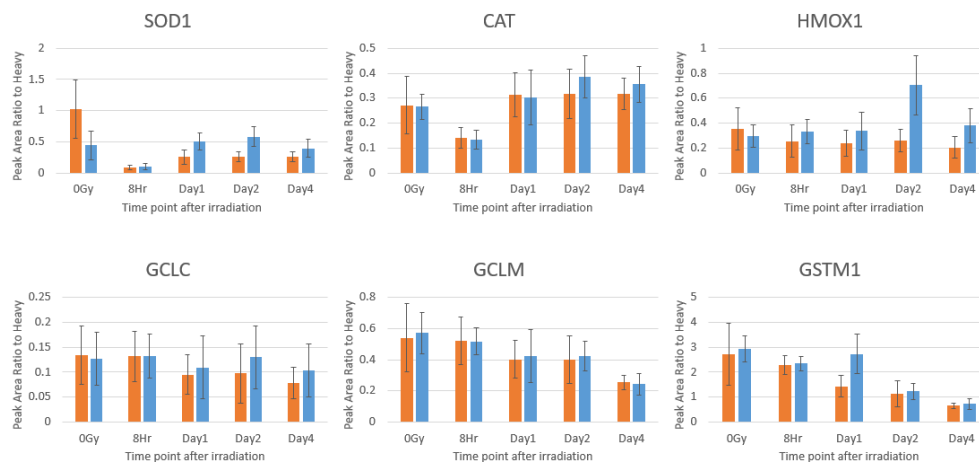


Figure 3.1: Time-dependent antioxidant enzyme response in mouse bone marrow (n=8) following 6 Gy TBI as represented by relative peak area ratios of endogenous to SIS peptides obtained from Skyline. (a) C57Bl/6 male (blue) and female (orange) mice, (b) C3H male (blue) and female (orange) mice. Error bars indicate standard errors of the mean ratios from both biological and technical replicates.

3.4.2 Statistical significant changes using MSstats

Skyline data were imported to MSstats in R to test the statistical significance of protein abundance changes at each time point relative to the unirradiated controls. Data were processed within individual mouse groups. MSstats first log₂-transforms and normalizes intensities in all runs by equalizing the median intensities of the heavy standard peptides. It then generates protein-level summaries for data visualization and quality control after imputation for missing values and removal of poor quality features. Among the visualization outputs generated in this step, a condition plot displays potential systematic differences in protein intensities between conditions (examples shown in Figure 3.2). Next, to find differentially abundant proteins, it applies intensity-based linear mixed effect models to determine estimate of protein abundance and variation.^[42] The heatmaps generated from this step provide convenient visualization for strain and gender comparisons (Figure 3.3).

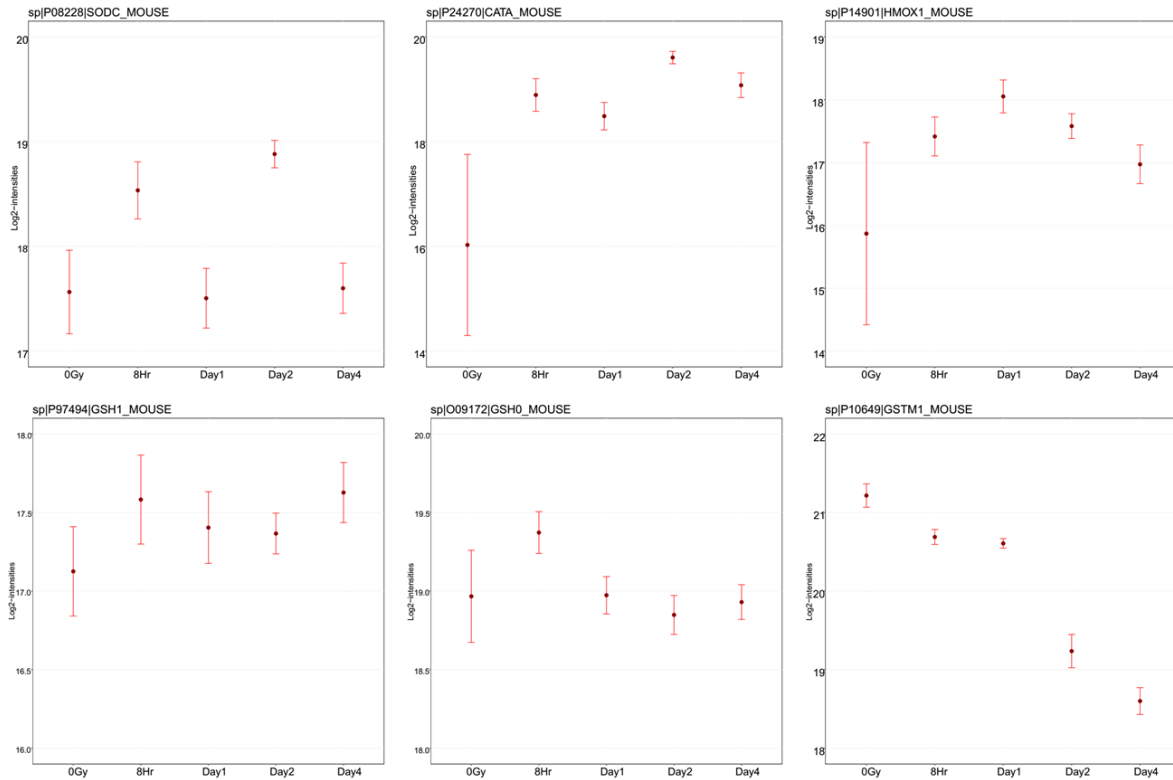


Figure 3.2: Condition plots for refined protein intensities in bone marrow of C57Bl/6 male mice after 6 Gy TBI. Dots indicate the mean of log2 intensities for each time point. Error bars indicate the confidence interval with 0.95 significant level for each time point.

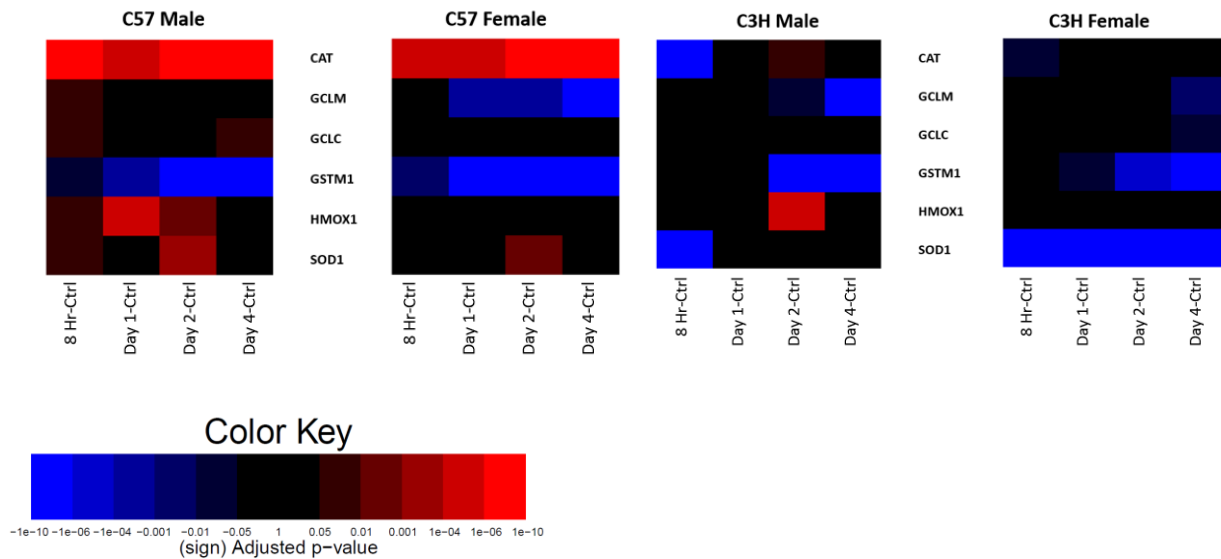


Figure 3.3: Statistically significance of protein changes in mouse bone marrow at 8 h, Day 1, Day 2, and Day 4 after 6 Gy TBI compared to unirradiated control in each strain/gender group (n=8). Columns in the heatmaps are comparisons of time points relative to control, and rows are proteins. The heatmaps display signed FDR-adjusted p-values using the Benjamini and Hochberg approach. Negative sign (blue) indicates down-regulation; positive sign (red) indicates up-regulation. Brighter color represents stronger differential abundance. Black color represents no significant differential abundance.

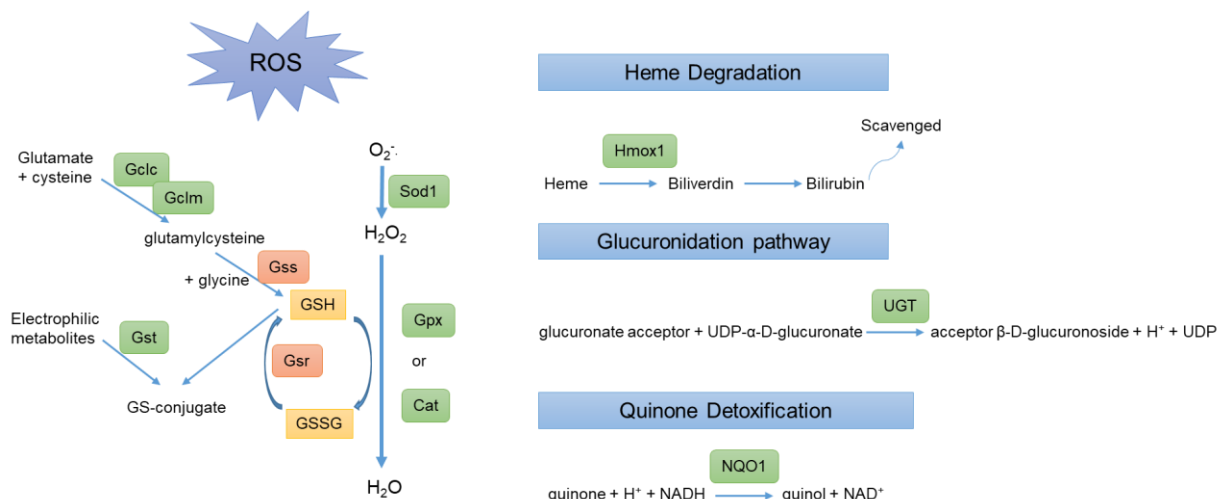


Figure 3.4: Schematic diagram of Nrf2 regulated antioxidants and xenobiotic pathways. The enzymes measured in this study are indicated by green boxes.

3.4.3 Time dependent radiation response in bone marrow

In general, the time course patterns for these proteins are surprisingly complex and reveal progressive changes in the response to radiation in the bone marrow. Specifically, the more frequently studied C57Bl/6 male mice showed elevation of CAT and HMOX1, a decrease in GSTM1 abundance, a biphasic pattern for SOD1, and no prominent change in two GCL subunits (Figure 3.2). With the expectation that higher antioxidant capacity is needed for cell survival after irradiation, it is surprising to see progressively decreased abundance of GST and GCL enzymes with time given their roles in glutathione homeostasis (Figure 3.4), which could be due to their overutilization. In contrast, SOD1 and CAT showed a biphasic response that differed in timing between the 2 mouse strains. For these, a nadir was seen at either 8 or 24 hr for most mouse groups (Figure 3.1), which is in keeping with the findings of the Romeo group.^[43] This biphasic theme that emerged may reflect early and late radiation responses controlled by different mechanisms.^[32] Cellular responses to radiation are multifaceted and persisting. After an initial oxidative insult, a broad range of basal and inducible antioxidant responses is

initiated as a cytoprotective shield. Following these early events, cells also undergo further waves of secondary ROS generation, DNA damage, and signaling. These further pro-oxidant responses can persist through multiple cell divisions and manifest differently in different subcellular context. Changes of these Nrf2 target enzymes in our time course data could potentially represent waves of different signals in the cells and their attempts to respond.

Another layer of complexity comes from different radiation sensitivities in different cell types. A high sublethal dose of 6 Gy causes a rapid depletion of cells in the bone marrow and peripheral blood.^[44] In bone marrow, highly proliferative hematopoietic progenitor cells are particularly sensitive and plunge after 6 Gy irradiation, whereas other hematopoietic and mesenchymal cells are more resilient. There is also mass immigration from bone marrow into the circulation, which profoundly alters its composition. This is evident in the color of tissues that ranged from red marrow in control mice to yellow marrow in irradiated mice. These changes and subsequent repopulation can potentially result in disproportionate shifts in protein levels and be impacted by different basal levels of these antioxidant enzymes in various cell types.

3.4.4 IR-induced alterations in Nrf2-ARE regulated protein targets

Glutamate-Cysteine Ligase (GCL) enzyme is a heterodimer composed of a modifier (GCLM) and a catalytic (GCLC) subunit that catalyzes the first and rate-limiting step in glutathione (GSH) synthesis (Figure 3.4). The rate of GSH synthesis is influenced by (1) amount and relative ratios of the two GCL subunits, (2) availability of its substrate, L-cysteine, and (3) extent of feedback inhibition of GCL by GSH.^[45] GCL is predominantly regulated by the Nrf2-ARE pathway at the transcriptional level.^[45,46] Nrf2 knockout mice

showed decreased levels of GCLC and GCLM expression.^[46] In our data, we observed progressive decreases in abundance of GCLM in C57 F and C3H M&F mice following 6 Gy irradiation, but no significant change in GCLC levels (Figure 3.3). In most tissues, GCLM is thought to be the more rate limiting component and to enhance the catalytic ability of GCLC.^[47,48] Many laboratories have reported a transcriptional induction in one or both of the GCL genes with a wide range of inducers in different cell types.^[49] It is possible that GCL activity is regulated post-translationally. One study reported that treatment of Jurkat cells with ionizing radiation and other model oxidants acutely activated GCL without affecting GCLC or GCLM protein levels. The report proposed a mechanism of post-translational activation whereby an increased proportion of GCL in the holoenzyme form compared to the inactive monomeric form results in high activity and GSH production.^[50] Another interpretation is that the high level of damage switches the redox rheostat towards a pro-oxidant inflammatory response.^[32] This second interpretation would suggest that this enzyme would be an ideal biomarker for assessing damage, and mitigators aimed at increasing its expression would be of value.

Glutathione s-Transferases (GSTs) are a large family of enzymes that conjugate glutathione to electrophilic centers on a wide variety of substances and are therefore involved in detoxification of xenobiotics. GSTs are highly polymorphic^[51] and different variants exist in different tissues.^[33] Within the GST superfamily, GST π is known to inhibit c-Jun N-terminal kinase (JNK) nonenzymatically to prevent JNK activation and apoptosis.^[52] Radiation-induced oxidative stress can block this interaction to induce apoptosis. GSTM1 can also regulate apoptosis through signal-regulating kinase (ASK1), which activates JNK and p38 pathways.^[53] Interestingly, in our experiment we observed

consistent decreases in GST Mu1 levels across strains and genders. The same pattern for GST was also observed in our discovery proteomic experiment from mouse bone marrow using the same irradiation treatment, in which GSTM1 and GSTP1 both progressively decreased over the course of 30 days after irradiation (data not shown). Similar findings for GST radiation response have been reported by other groups. Cholon *et al.* observed an initial decreased level of GST activity and in cytosolic GST pi isoform in CHO cells after 4.5 Gy of ionizing radiation.^[54] In their study, they only examined π and α isoforms of GST and they classified π isozyme as an early response gene to ionizing radiation. Adams *et al.* also found lower *in vivo* mouse bone marrow GST levels after 2 Gy.^[55] They also discovered that the major changes in GSH and GST occurred in the granulocytes of the bone marrow.^[55] Based on these results, GST protein is radiation responsive and potentially dose-dependent. Furthermore, GST isoforms are tissue-specific, which suggests it to be a desirable biomarker candidate for tissue-specific diagnosis.

Heme oxygenase 1 (HO-1) is an inducible enzyme that catalyzes degradation of heme to biliverdin, CO, and iron. Heme oxygenase is abundant in tissues that degrade aged red blood cells, such as the spleen, liver and bone marrow. When red blood cells are lysed, free heme is released and can cross cell membranes to cause oxidative stress.^[56] By breaking down toxic heme, HO plays a critical role in vascular biology, iron recycling and cellular protection against oxidative stress.^[57] In the context of radiation, HO-1 and CO are found to participate in DNA-repair through the ATM protein.^[58] In our data, HO-1 peaked at Day 1-2 for C57 male mice and Day 2 for C3H male mice (Figure 3.1). McDonald *et al.* found a dose-dependent increase in HO-1 mRNA expression as

well as protein level in mouse embryonic fibroblast cells irradiated daily with 0.5, 2, or 4 Gy for 5 days.^[30] They further tested *in vivo* response, in which they also observed a significant increase in HO-1 levels in the spleens of C57Bl/6 mice irradiated with 2 Gy whole body every 24 hours for 5 days.^[30] For HO-1, there seems to be good correlation between mRNA expression and protein levels, which suggests the protein level changes are primarily caused by transcriptional activation by ionizing radiation.

Superoxide dismutase (SOD1) and catalase (CAT) work coordinately to scavenge and detoxify reactive oxygen species and are essential for antioxidant defense in radiation responses. SOD1 converts free radicals to hydrogen peroxide, and CAT then breaks down H₂O₂ to H₂O. As such they are involved in apoptosis and cell death. SOD1 is present in the mitochondria and cytosol of virtually all eukaryotic cells and catalase is mostly located in peroxisomes. For these two enzymes, we observed complex wave-like patterns in response to radiation. Besides catalase, glutathione peroxidases (GPX) also detoxify H₂O₂, and the relative contribution of CAT and GPX to H₂O₂ removal is cell type and tissue dependent.^[59] The relationships between these antioxidants is further complicated by induction of SOD1 through pro-inflammatory pathways that could be involved in our experiments.^[32]

3.4.5 Gender and strain differences in radiation response

Both strain and gender differences were detected from our protein measurements. It is known that genetic variations in a population contribute to considerable differences in radiation response.^[60–62] Previously, Wright's group observed genotype-dependent responses in bone marrow from C57Bl/6 and CBA/Ca strains after 4 Gy γ -irradiation;^[63] they explained the differences in response as a result of different bone marrow

macrophage activities, in which CBA/Ca tissue showed damaging inflammatory-type response, whereas C57Bl/6 bone marrow showed anti-inflammatory or protective response.^[64] Taking this diversity in radiation response into account, a consensus has been established by the radiation medical countermeasure community to test more than one mouse strain in development of radiation protectors and mitigators.^[65] Specifically, C57Bl/6 and C3H/HeN strains are recommended, for which the most data are available and divergence in tissue responses to radiation has been demonstrated.^[65] C57Bl/6 mice are more radioresistant to hematopoietic ARS than C3H mice, which can be explained by more common myeloid progenitor cells in the bone marrow, and in our data they also gave a stronger response of Nrf2-regulated antioxidant proteins to 6 Gy TBI.

A few radiobiology studies have reported gender difference in radiation sensitivity. In our study, within each strain, male mice appeared to have more occurrences of upregulation of these antioxidant enzymes than female mice. The most prominent example is HO-1, in which male mice of both strains showed upregulation in either Day 1 or Day 2 whereas female mice did not (Figure 3.3). A recent study investigated gender differences in genome damage in prepubertal and adult mice following 8 Gy gamma radiation using an *in vivo* micronucleus assay.^[66] Irradiation caused higher frequency of micronuclei in males of both age groups.^[66] Other studies have also shown that male mice sustained more radiation damage than female mice given the same exposure.^[67,68] Sex hormones, particularly estrogen, have been suggested to play a radioprotective role. Interestingly, a more fundamental study has looked at the inherent difference in cell death programs between the genders.^[69] The authors proposed that male mice are more prone to PARP-1 necrosis (inflammatory cell death), whereas female mice are more prone to

cascade-dependent apoptosis (non-inflammatory cell death) and that estrogen mediates this gender-biased cell death.

The trend of gender difference in radiation sensitivity seems to be translatable from mice to human. Although very few clinical studies on gender-specific differences in radiation sensitivity are available, a number of epidemiological studies have reported such differences in radiation-induced cancer incidence and mortality. In the Life Span Study of atomic bomb survivors, women were found to have a significantly lower risk than men in development of radiation-associated leukemia.^[70] To draw more definitive conclusions about gender differences in radiation response, more systematic radiobiological studies using various cell or animal models of both genders are needed.

3.5 Conclusion

This study reveals time dependent changes in Nrf2-regulated proteins in mouse bone marrow following 6 Gy whole body irradiation in representative mouse strains of both genders. Despite the complexity of the bone marrow tissue environment, we observed some prominent patterns. Among these, the most consistent trend across all mouse models is the decreased abundance of glutathione S-transferase Mu1 isoform. GSTM1 and related isoforms appear to be promising biomarker candidates and their radiation response in blood plasma and dose dependency should be further evaluated. Other patterns, including biphasic responses, are strain or gender-specific.

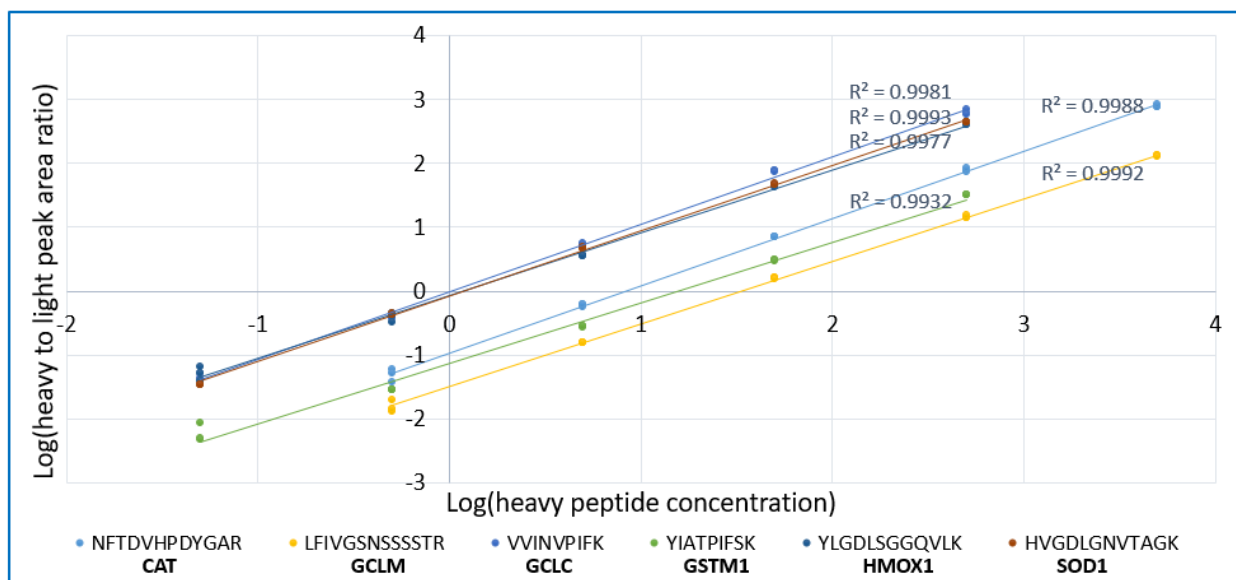
An ideal radiation injury biomarker should satisfy the following criteria. First, it should be readily obtainable (e.g. serum, urine, saliva, sweat); second, the response should be radiation dose-dependent; third, it should be persistent during the triage timeframe; last, the response should be radiation-specific and not confounded by other

stressors. Nrf2-regulated proteins have the potential to fulfill these requirements based on previous experimental evidence of robust and dose-dependent activation following IR and importance of this pathway in radiation response.^[30,31] Beyond the set of Nrf2-regulated proteins measured in this experiment, other Nrf2-induced proteins are worth investigating in future experiments for their biomarker potential, such as the proteins encoding the genes that were potentially induced in the recent transcriptional study by Purbey *et al.*^[31]

Given that bone marrow is the major blood forming organ, this result can be indicative of detectable changes in blood. This study establishes a targeted MS workflow and provides the basis for future development of organ-specific protein biomarkers used in diagnostic blood test for radiation injury. We acknowledge that these potential markers discovered from tissue will be highly diluted once in the blood stream. To target low abundance protein biomarkers in blood, antibody enrichment strategies may be needed, such as affinity capture of either intact proteins from larger volumes of blood or of peptides using peptide-directed antibodies (e.g., Stable Isotope Standards and Capture by Anti-Peptide Antibodies or SISCAPA).^[71] SISCAPA combines the sensitivity of antibody enrichment with the specificity of targeted MS detection, offering a solution to bridge discovery and validation of biomarkers, which is beyond the scope of the current study.

Biomarkers for radiation injury not only serves diagnostic or predictive purposes for triage, they are also extremely valuable in radiation countermeasure drug development, in which typical human clinical trials for radiation is not possible and biomarkers are needed to reflect mitigation effects and demonstrate efficacy of new drugs.^[3]

Supplementary Figures



S3.1: Linear response curve by spiking varying heavy standard peptide concentrations in a constant endogenous sample matrix consisted of pooled C57Bl/6 male control mice digest samples. The final heavy peptide concentrations in the pool were either 0.05, 0.5, 5, 50, 500 nM or 0.5, 5, 50, 500, 5000 nM depending on the peptide (the range was adjusted to match concentrations of endogenous peptides).

Raw data and Skyline data repository access

Thermo raw files have been deposited to PeptideAtlas with the dataset identifier:

PASS01319 (<http://www.peptideatlas.org/PASS/PASS01319>)

Skyline files have been deposited to Panorama and can be accessed from

<https://panoramaweb.org/pLlaWf.url>

CHAPTER 4: TARGET IDENTIFICATION OF NOVEL RADIATION MITIGATORS IN DEVELOPMENT

4.1 Abstract

The limited availability of FDA-approved radiation countermeasures for treatment of acute radiation syndrome (ARS) represents a significant unmet medical need. Researchers at the UCLA CMCR has recently identified a novel group of small molecule compounds from high throughput screening for inhibitors of radiation-induced apoptosis. This group of compounds shares a 4-nitrophenylsulfonamide (NPS) backbone. The lead compound not only dramatically decreases mortality from hematopoietic ARS in mice, it also provides mitigating effect in radiation injury in other tissues. The mechanism of action for the lead compound needs to be determined to advance the drug development. To facilitate this process, I adopted a thermal proteome profiling (TPP) approach to discover hypothetical targets for this drug candidate. TPP is an emerging method in phenotypic-based drug discovery that allows for an unbiased search for drug targets on a proteome wide scale. TPP is based on the principle that proteins become more resistant to heat upon ligand binding. In the first experiment, a conventional TPP method was applied in which cell lysates were incubated with the Compound 512 or DMSO control, and then subjected to 10 temperature treatments. A total of 7322 proteins with thermal stability data were obtained from this TPP experiment. Twelve proteins showed significant melting curve shifts according to the criteria set by the original developer of the workflow, and half of these proteins showed stabilization by the compound. In the second experiment, a new high-throughput approach named Proteome Integral Stability Alteration (PISA) was adopted, in which temperature treatments were pooled and the integral stability between

control and drug treatment was compared. Since there is no published protocol for PISA yet, it is still in exploratory phase. Based on my preliminary data, I discussed some considerations in data quality checks and raised concern on reproducibility of these types of experiments.

4.2 Introduction

Radiation Countermeasure Development

Despite the increasing threat of unexpected radiation exposure from terrorism, there is a dearth of FDA-approved radiation countermeasures for treatment of acute radiation syndrome (ARS). Neupogen (G-CSF) is the first FDA-approved radiomitigator to increase survival in patients exposed to myelosuppressive doses of radiation, or hematopoietic-ARS.^[6] It was approved by the FDA based on animal studies because human clinical trials could not be ethically conducted. Later, Neulasta (PEGylated G-CSF) and Leukine (GM-CSF) were also approved by the FDA for treatment of H-ARS.^[7] All three radiomitigators work similarly by accelerating neutrophil recovery, and they are only approved for the treatment of the H-ARS subtype.

Recently, a novel group of small molecule compounds has been identified from high throughput screening for inhibitors of radiation-induced apoptosis.^[8] The group of compounds with 4-nitrophenylsulfonamide (NPS) backbone emerged from in vitro high-throughput screening (HTS) for inhibitors of apoptosis (Figure 4.1). A compound library of 85,000 molecules were screened in pre-irradiated (2 Gy) TIL1 lymphocytic cells that are sensitive to radiation apoptosis. Cell viability was assessed comparing drug-treated to irradiated control cells. A hit from the in vitro assay is defined as >130% increased viability compared to irradiated control. A major group of the top hits from this in vitro screening shares the NPS scaffold. Among the 10 NPS compounds shown in Figure 4.1, 8 of them were tested in vivo, in which the compounds were administered via subcutaneous injection to the mice 24 h after 7.725 Gy irradiation (LD70/30) daily for 5 days. The top 3 hits from in vivo testing are Compounds #3, 4, 5 in Figure 4.1. From the

survival plots, we can see these 3 compounds showed significant improvement of survival at 3 different dosing levels, contrasting to Compound #1 that showed little efficacy. Among these 3 molecules, Compound #5 or 512 is assigned as the lead compound. It is not only able to mitigate hematopoietic ARS, but is also effective at mitigating radiation injury from other organs such as gut, thorax, and lung. This broad spectrum mitigation effect is highly desirable because the current FDA-approved ARS mitigators only act on hematopoietic ARS. Moreover, the lead compound has low toxicity and anti-tumor action.

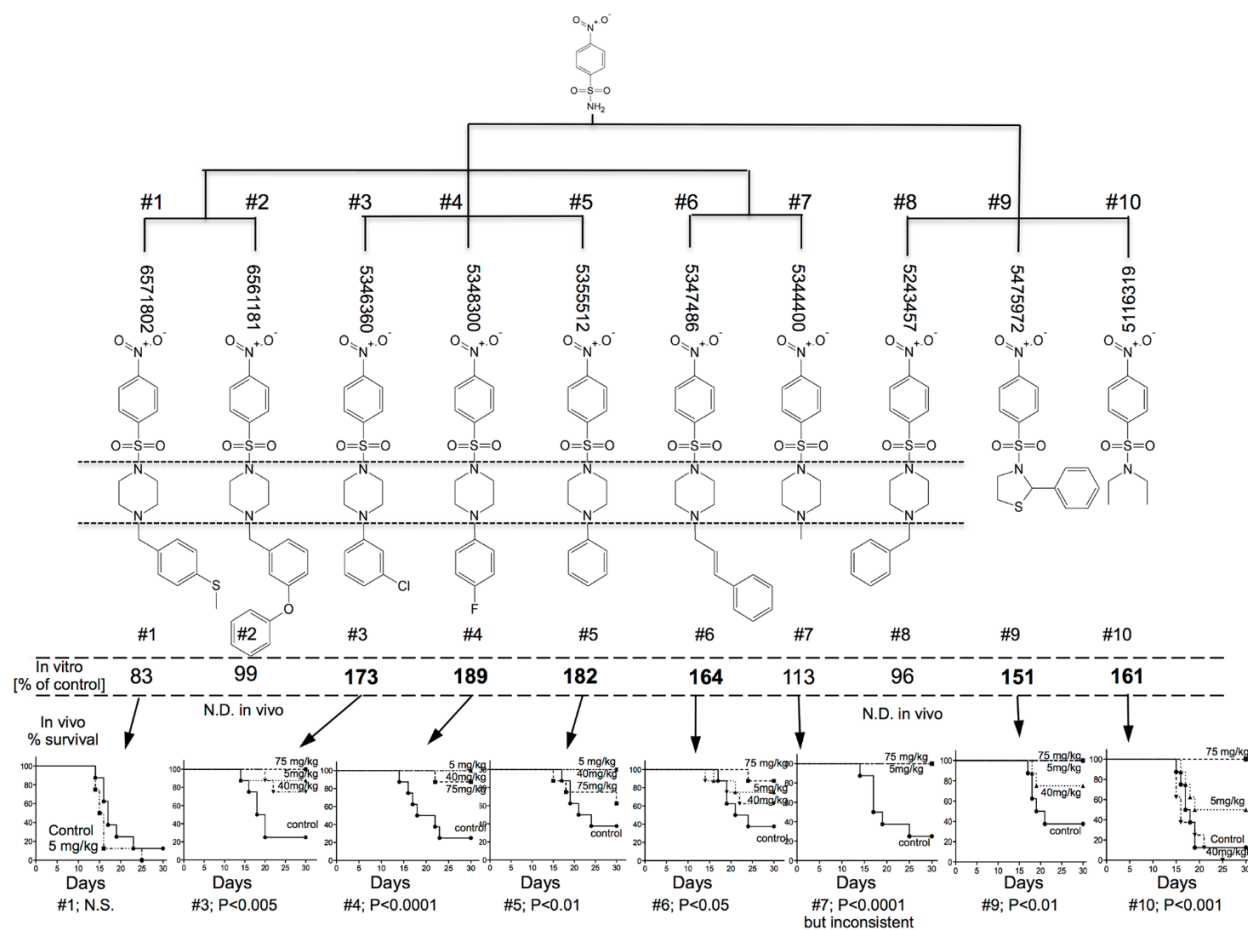


Figure 4.1: In vitro and in vivo results of 4-(nitrophenylsulfonyl)piperazines (NPSP, #1-8) and 4-nitrophenylsulfonamides (NPS, #9-10) compounds. In in-vitro screening, compounds were verified as “hits” if they blocked radiation-induced apoptosis in an annexin V/PI flow cytometry assay. The data underneath each compound refers to % viability of TIL1 lymphocytic cells at 24 hrs, compounds being added at 10 μ M to TIL1 cells 1 hr after 2 Gy irradiation. Viability was assessed by ATPLite production at 24 hrs and is shown relative to 100% of irradiated controls, with >130% (bold) being taken as a significant increase. All except #1 and #8 were tested in vivo (bottom graphs). They were injected in 1% Cremophor s.c. into C3H male mice (8 per group) starting 24 hrs after 7.725 Gy WBI (LD70/30 estimate), daily for 5 days. Survival to the day 30 endpoint is expressed using a Kaplan-Meier plot with log rank statistics.^[8]

Target Identification for Mechanism Elucidation

The mechanism of action for the lead compound remains to be determined to advance the drug development process. There is some evidence suggesting that the drug might act through some primitive development pathways such as the Wnt or Hedgehog-Gli signaling pathway. To uncover the molecular mechanism of the lead compound (512), we adopted the thermal proteome profiling (TPP) approach to discover cellular targets for this drug candidate. TPP is a proteome-wide target identification approach that is based on thermal shift assay. In the Cellular Thermal Shift Assay (CETSA), protein samples are heated to a range of temperatures during which they unfold and form aggregates. Ligand binding typically stabilizes the protein structure and increases the unfolding temperature, hence we observe a right shift in the melting curve with drug treatment (Figure 4.2^[72]). Early CETSA work uses Western blotting as the readout, which limits the number of proteins analyzed in one experiment.^[73] CETSA was later combined with multiplexed quantitative mass spectrometry into a new workflow, termed Thermal Proteome Profiling or TPP (Figure 4.3^[74]). Quantitative MS makes it possible to assess thousands of proteins in parallel for thermal stability perturbation by ligand binding.

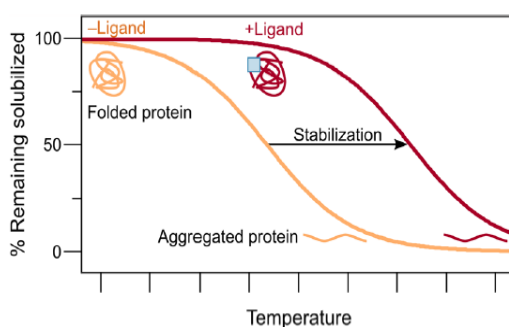


Figure 4.2: Principle of thermal shift assays. Proteins can be thermally stabilized by a ligand, leading to higher apparent melting temperature.^[72]

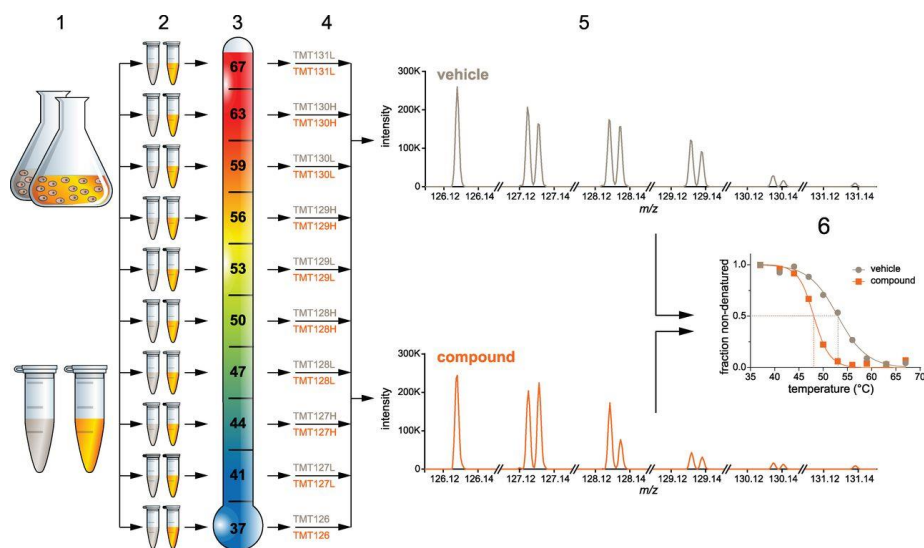


Figure 4.3: Schematic of a typical TPP experiment with TMT10 labeling. The reporter ion intensities were used to fit the melting curve and calculate the melting temperature (T_m) of each protein for vehicle or compound treated condition.^[74]

TPP is the first published methodology that allows mass spectrometry-based proteome-wide profiling for comprehensive target identification, and it is regarded as a major step forward in drug discovery research.^[75] Phenotypic screening-based drug discovery has been the popular approach in recent decades, whereby large numbers of compounds are screened for a desired biological response.^[76] This approach has the benefit of preserving cellular or organism-based context of protein function, however, they require follow-up studies to determine the precise protein target(s) responsible for the observed phenotype.^[76] The conventional approach to finding target proteins that bind to small molecules is affinity purification. Typically in this approach, the compound is derivatized and immobilized to a column, and then cell extracts are loaded to the column with the expectation that protein targets bind and elute after wash steps. The main caveat for this approach is that when the compound is derivatized and bound to a solid support, its interaction with the target proteins might be adversely affected. Other challenges with affinity based approaches are possible non-specific interactions and loss of true binders

due to stringent wash conditions used. As a result, this method works best for high affinity ligands binding to abundant targets. More recent affinity based methods have attempted to overcome some of these challenges, but they involve additional chemistry reactions that add other biases and cost to the process. On the contrary, TPP is an emerging approach that avoids compound derivatization and directly monitors a response from ligand binding in a physiologically relevant setting. This approach can also be applied to living cells besides cell extracts to uncover indirect targets or downstream effects of the drug in living cells.

Two types of TPP experiments were initially proposed by Savitski's group: TPP-TR (temperature range) experiment, which is performed over a temperature range at a fixed compound concentration, and TPP-CCR (compound concentration range), which is conducted at a single temperature over a range of compound concentrations (Figure 4.4^[75]). The TPP-CCR is also known as the isothermal dose-response (ITDR) experiment, whereby compound potency can be determined.

Specifically, in a typical TPP-TR experiment, cells or cell extracts are first treated with vehicle or drug. Samples are divided into 10 aliquots and subjected to heating at various temperatures (e.g. 37-67°C). Each sample is digested with trypsin and labeled with the TMT10 isotope tag. Samples from each condition (vehicle, drug) are mixed prior to LC-MS/MS analysis. Protein identification and quantification is performed. Melting curves for all quantifiable proteins are generated. Melting points (T_m) for vehicle- and drug-treated conditions are compared, and proteins with significantly altered T_m 's are identified as potential targets. These targets can be further validated with TPP-CCR experiments. In the TPP-CCR experiment, cells or cell lysates are treated with vehicle or

drug over 9 concentrations. These 10 samples are subjected to heating at the same temperature, which is carefully chosen to include the T_m 's of the potential targets. Samples are again digested with trypsin and labeled with TMT10 prior to analysis. After protein identification and quantification, dose response curves are fitted and pEC_{50} values (negative log of the concentration at which 50% of the total stabilizing effect has been observed) are calculated for proteins whose thermal stability is affected by the drug.

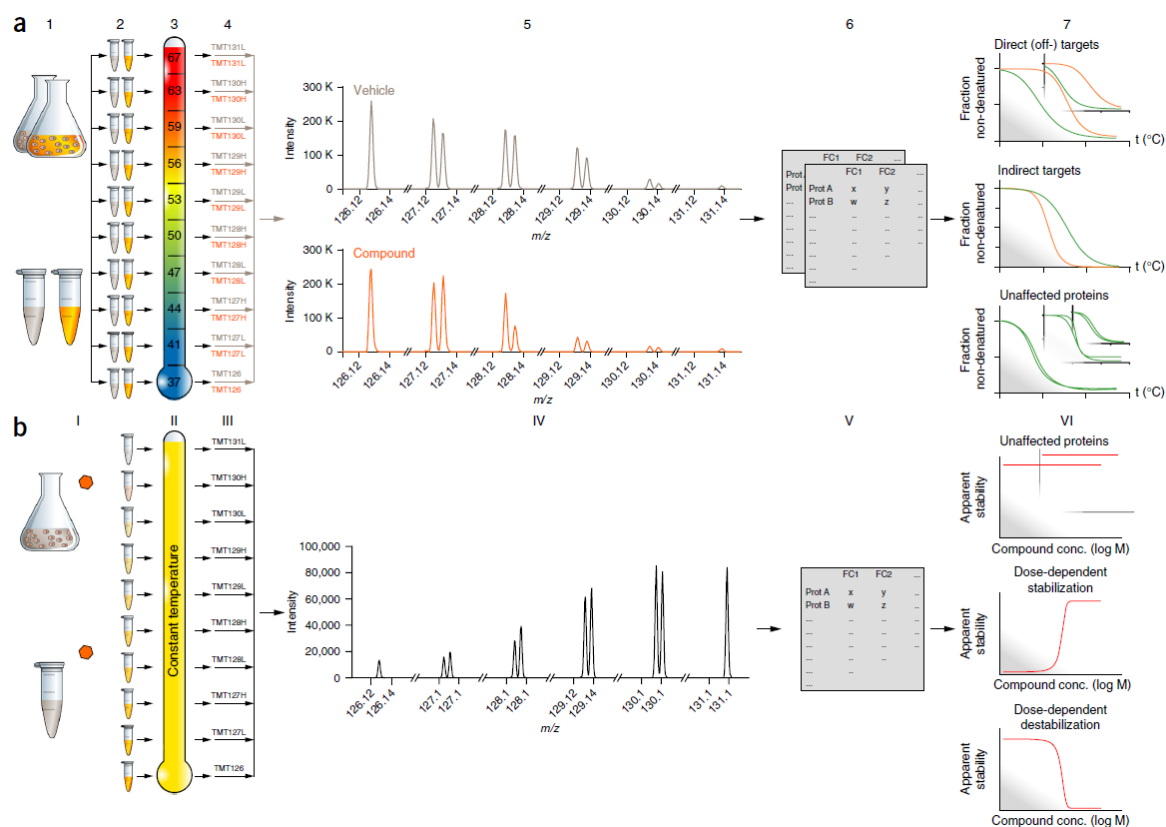


Figure 4.4: TPP experiment schematic. (a) TPP-TR experiment. (b) TPP-CCR experiment.^[75]

In my TPP-TR experiment, I used the software package downloaded from the Nature Protocol published by Savitski's group (Figure 4.5).^[75] The first step of the workflow is a python package that generates protein ID's and quantification using Mascot. The software merges results from multiple fractions and generates protein level

summaries. These summaries are then processed in R to create melting curves and identify significant shifts in melting curves primarily based on shifts in T_m 's.

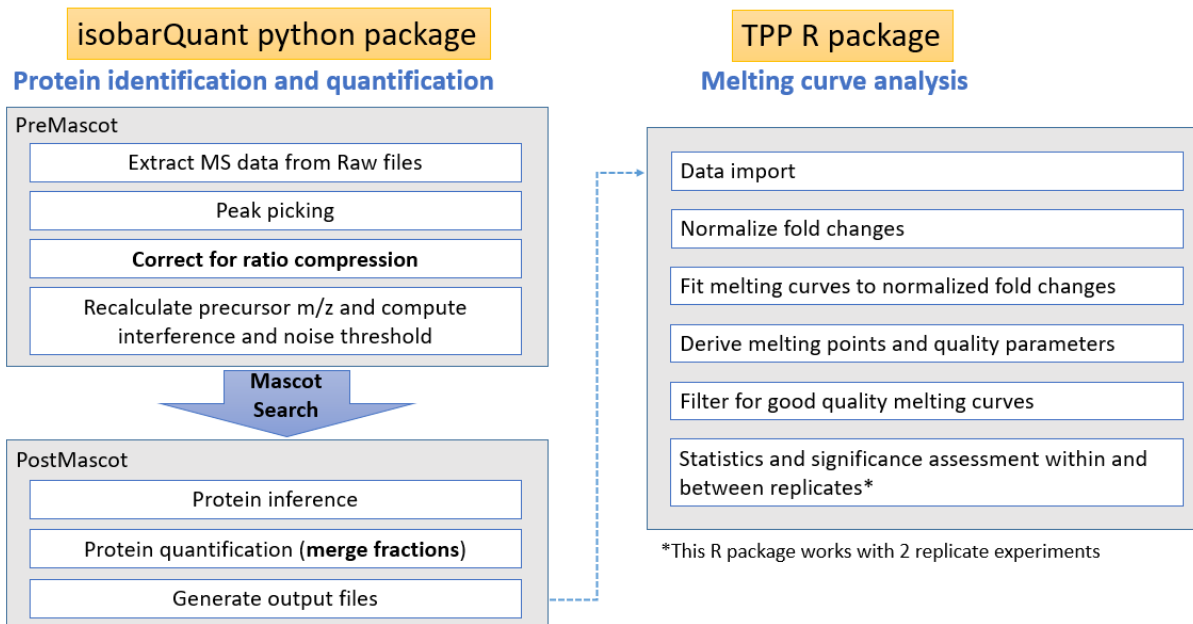


Figure 4.5: Software package for melting curve analysis in TPP experiment.

To generate melting curves, the fold change of protein abundance at each temperature treatment relative to the lowest temperature is calculated, and fitted to a sigmoidal curve based on the formula derived from chemical denaturation theory (Figure 4.6). The critical parameters used for filtering and significance calculations are (1) T_m (melting point of a protein), which is defined as temperature at which half of the proteins is denatured, and (2) R^2 , coefficient of determination, which describes how well the fold changes fit the melting curve. The software has a cutoff for Plateau (<0.3) and R^2 (>0.8) values to filter for good quality melting curves. These melting curves are then subjected to final 4 requirements for significant shift, and proteins that pass the following criteria are the proposed targets from this workflow:

(1) p-value < 0.1 or 0.2 ; p-value is computed from z-test with correction for multiple testing (Benjamini-Hochberg);

- (2) melting curves of two replicates should shift in the consistent direction;
- (3) the magnitude of the T_m shift between drug treatment and control should be greater than difference between the two control replicates;
- (4) slope has to be steeper than -0.6 (steeper slope is found to give more reproducible melting point).

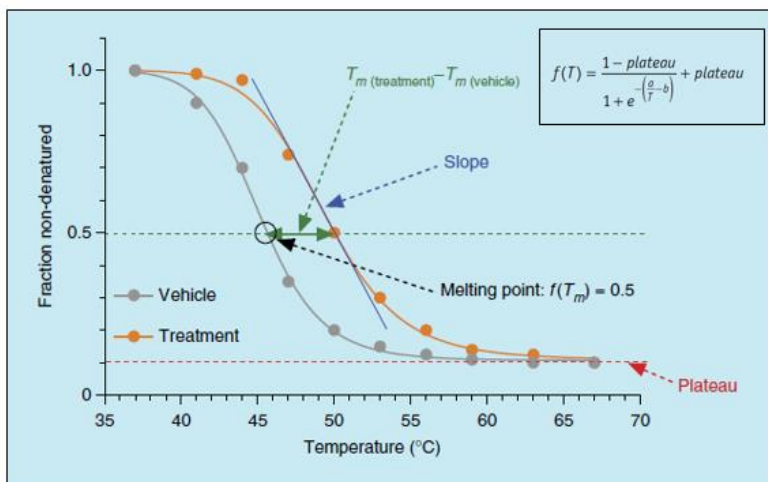


Figure 4.6. Melting curve schematic. Fraction non-denatured is computed from fold change of protein abundance at each temperature relative to lowest temperature (e.g. 37°C). These fold changes are fitted to a sigmoidal curve based on the formula shown in the upper right insert. T_m is defined as temperature at which half of the proteins are denatured. Thermal stability shift is represented by $T_m(\text{treatment}) - T_m(\text{vehicle})$.^[75]

In a theoretical TPP-CCR experiment, fold changes at different compound concentrations relative to vehicle are computed. These fold changes represent the protein's apparent stability at the specified concentration. A fold change $>3/2$ is designated as stabilization by the compound, and conversely, a fold change $<2/3$ is regarded as destabilization by the compound. If a protein is proposed as a target in a TPP-TR experiment, but shows no dose-dependent behavior in a TPP-CCR experiment, it is likely a false positive. Another sigmoidal curve formula is used for curve fitting (Figure 4.7a). In this formula, EC_{50} is the compound concentration at which the value of the fitted curve is 0.5 (Figure 4.7b). Proteins that show significant dose-dependent changes in

thermal stability in response to drug treatment are validated as real hits from TPP-TR experiments.

a)

$$Y = \frac{1}{1 + 10^{(\log EC_{50} - x) \text{ slope}}}$$

b)

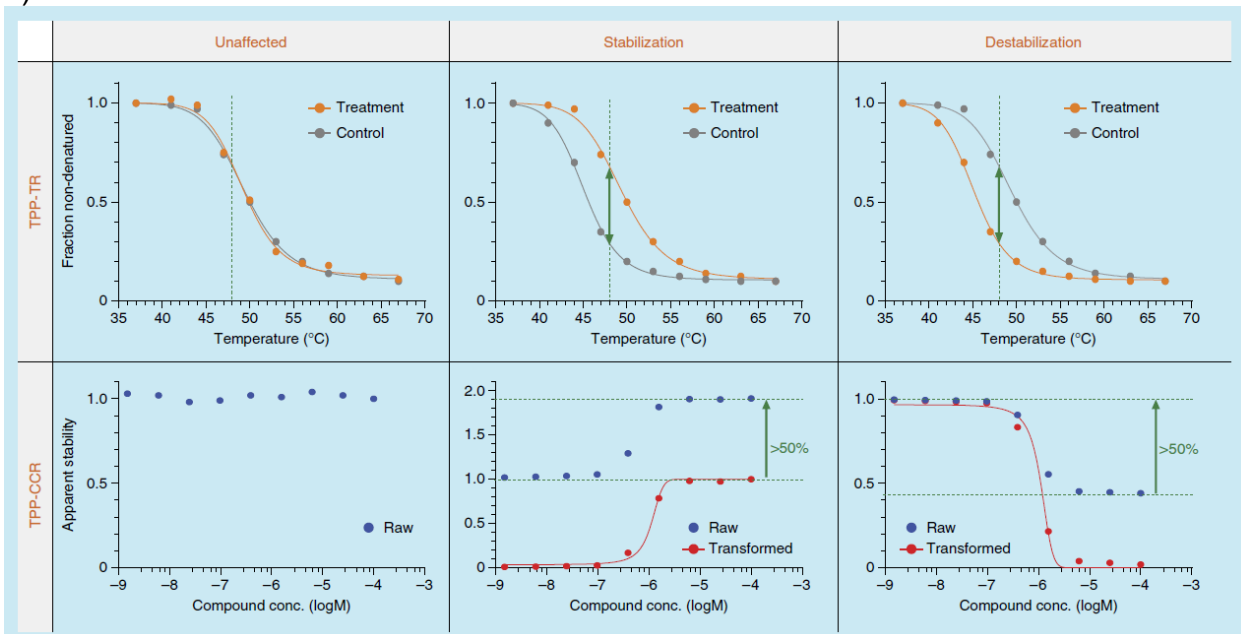


Figure 4.7: TPP-CCR curve fitting formula (a) and dose response curve schematic (b). The temperature should be chosen to maximize the offset between vehicle- and compound-treated melting curves in the corresponding TPP-TR experiment. The range of concentrations should go from 0 to saturating concentration.^[75]

New TPP Methodology - Proteome Integral Stability Alteration (PISA)

After early publications of TPP by Savitski's and Nordlund's groups, newer TPP workflows have arisen in the literature that aims to simplify or streamline this process. One promising workflow is the Proteome Integral Stability Alteration (PISA) proposed by Zubarev's lab.^[77] Their PISA approach achieves higher throughput and lower cost compared to the conventional TPP workflow by pooling all the temperature treatments into one combined sample and comparing the "integral" stability between drug and control conditions (Figure 4.8, Figure 4.9). By processing the combined sample, this PISA

workflow greatly reduces sample preparation complexity and variation. An additional benefit of PISA is that it is not dependent on melting curve fitting as for the conventional TPP workflow where stringent curve fitting criteria are imposed that results in loss of many proteins from being considered for the statistical testing. The number of false negatives is potentially reduced using the PISA approach. Because of the predicted increase in sensitivity, specificity and throughput of PISA approach, I also performed this PISA workflow using the same cell lysates as the conventional TPP experiment, and compared the results.

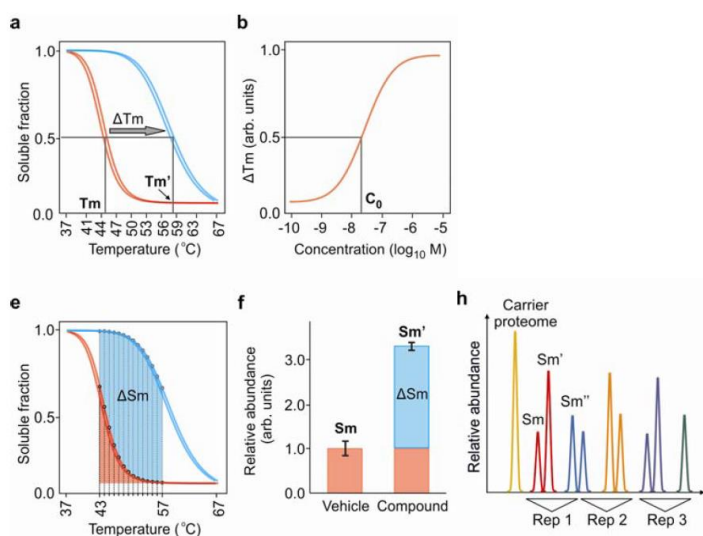


Figure 4.8: Traditional TPP vs. PISA data analysis. (a) TPP-TR melting curve (b) TPP-CCR dose response curve (e)(f) PISA data representation, measuring ΔS_m as a difference between the integral abundances of the protein in the treated and untreated samples (h) Example of a TMT-labeling scheme for a triplicate 2D PISA experiment, where S_m is the control sample, S_m' is drug-treated with saturating drug concentration, S_m'' is drug-treated sample with moderate drug concentration.^[77]

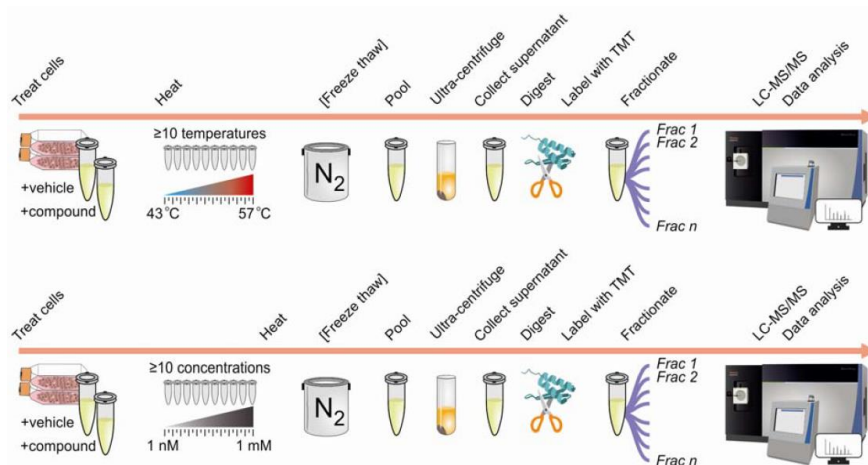


Figure 4.9: PISA experiment workflow schematic. Control or drug-treated sample is divided into 10 aliquots and subjected to 10 different temperature treatments (top) or drug concentrations (below). The 10 samples are pooled before ultracentrifugation and following digestion steps. The two pooled samples are labeled with TMT and fractionated prior to LC-MS/MS.^[77]

4.3 Materials and Methods

4.3.1 Conventional TPP experiment

Cell Culture and Lysis

Mouse tumor infiltrating lymphocytes (TIL) cells were grown in RPMI [+] L-glutamine and additionally supplemented with 10% fetal bovine serum and 1% 100X antibiotic antimycotic solution at 37°C, 5% CO₂. Approximately 120 million TIL cells were harvested for each TPP experiment and washed with PBS. Two biological replicates of the TPP experiment came from cells harvested on two different days. The cells were suspended in 1.2 ml lysis buffer containing 100mM Tris-HCl, 150mM NaCl, 0.1% NP-40 (IGEPAL® CA-630, Sigma Aldrich), Roche complete mini Protease inhibitor (1 tablet dissolved in 500 µl H₂O), and Thermo HALT phosphatase inhibitor cocktail (100 µl) on ice. The cell suspensions were freeze-thawed 3 times by using liquid nitrogen. The soluble fraction was separated from the cell debris by centrifugation at 16,000 g for 10 min at 4

C. Protein concentration from the lysate was estimated by the BCA quantitation assay (Thermo Pierce).

Drug Incubation and Heat Treatment

The cell lysate was diluted with more lysis buffer to a final concentration of ~2mg/ml and then divided into 2 aliquots of 594 μ l each. One aliquot was treated with 6 μ l of DMSO and the other was treated with 6 μ l of 1 mM Compound 512 (10 μ M final concentration). After gentle mixing of each tube, they were incubated at room temperature for 30 min.

After drug incubation, the lysates were further divided into 10 PCR tubes of 55 μ l aliquots. These 20 aliquots were heated for 3 min on a PCR machine (BioRad C1000 Touch™ Thermal Cycler) with a temperature gradient setup (37, 41, 44, 47, 50, 53, 56, 59, 63, 67 °C), followed by a cool down at 4°C for 3 min. The heated cell lysates were ultracentrifuged at 100,000 g (48,000 RPM for TLA 100 rotor on a Beckman Coulter Optima™ TLX ultracentrifuge) for 20 min at 4°C, and 45 μ l supernatants were collected without touching the pellet. Protein concentration of each sample was determined by the BCA assay.

MS Sample Preparation

Proteins were precipitated by adding 4X volumes of cold acetone (140 μ l) and cooled for 2 hours at -20°C. The supernatants were removed by centrifugation at 8000 g for 10 min. When acetone was mostly dried out, the pellet was resuspended in 100 μ l membrane compatible buffer containing 50mM triethylammonium bicarbonate (TEAB) with 0.5% sodium deoxycholate, and 12 mM sodium lauryl sarcosine. The proteins were denatured by sonication for 5 min, followed with heating at 95°C for 5 min. Disulfide bonds were reduced by tris(2-carboxyethyl)phosphine (TCEP) to a final concentration of 5 mM

at room temperature for 30 min. Cysteine residues were alkylated by iodoacetamide (12.5 mM final concentration) at room temperature in the dark for 30 min. The sample was diluted 5 fold with 50 mM TEAB. Proteins were digested by MS Grade trypsin with a 1:50 enzyme: protein ratio and incubated at 37°C overnight.

Peptides were acidified with trifluoroacetic acid (TFA) to a final concentration of 0.5% and vortexed for 5 min. To each sample, ethyl acetate (1:1 v/v) was added for detergent removal and vortexed for 5 min. The mixture was centrifuged at 12,000 g for 10 min, and the upper organic phase was removed. The ethyl acetate extraction was repeated once. Samples were desalted with C18 Micro spin columns (17-170ug capacity, Nest Group). Peptide concentration from each sample was determined by a fluorescent peptide quantitation assay (Pierce).

For TMT labeling, peptide samples were resuspended in 100 µl 200mM HEPES (4-(2-hydroxyethyl)-1-piperazineethanesulfonic acid), 30% ACN. To each TMT10plex label, 41 µl ACN was added to dissolve the tags for 5 min with occasional vortexing. Half of the sample (50 µl) was labeled with half of the TMT reagent (20 µl). The remaining half of sample was stored away. The labeling reaction went on for one hour and was quenched with 6 µl 5% hydroxylamine (in 200 mM HEPES) for 15 min, followed by acidification to 5% formic acid. The 10 samples from control or drugged treatment were combined. The two pooled samples were fractionated using the Pierce High pH Reversed-Phase Peptide Fractionation Kit following the manufacturer's protocol. Step elutions of increasing acetonitrile concentrations were performed to generate 8 fractions for LC-MS/MS analysis.

Liquid Chromatography–Mass Spectrometry

The digested peptides were dried and resuspended in 20 μ l 5% formic acid, and 2 μ l was injected onto a 25 cm by 75 μ m fused silica capillary column packed in-house with bulk C18 reversed phase resin (1.9 μ m, 100 Å pore, Dr. Maisch GmbH). A 140-minute water-acetonitrile gradient was applied on a Dionex Ultimate 3000 UHPLC system (Thermo Fisher Scientific) at a flow rate of 300 nl/min: at 0 min, 1% B; at 5-128 min, 5.5% B ramp to 27.5% B; at 135 to 136 min, 35% B ramp to 80% B; hold 80% B till 138 min; 138.5-140 min, equilibrate to 1% B (Buffer A: water with 3% DMSO and 0.1% formic acid and Buffer B: acetonitrile with 3% DMSO and 0.1% formic acid). Peptides were ionized by the application of a distal 2.2 kV and introduced into the Orbitrap Fusion Lumos mass spectrometer (Thermo Fisher Scientific).

The Orbitrap Fusion data acquisition method was set to the following: All MS1 spectra were acquired over m/z 300–1200 in the Orbitrap (120 K resolution at 200 m/z); automatic gain control (AGC) was set to accumulate 2E5 ions, with a maximum injection time of 100 ms. Data-dependent MS/MS analysis was performed using HCD in the Orbitrap. The normalized collision energy was optimized at 35% for HCD. MS² spectra were acquired with a fixed first m/z of 100. The intensity threshold for fragmentation was set to 4000, and included charge states 2+ to 6+. A dynamic exclusion of 25 s was applied with a mass tolerance of 10 ppm.

Data Analysis

Raw data were first processed in Thermo Proteome Discoverer 2.2 for verifying TMT labeling efficiency and overall data quality. For actual analysis, raw data were processed with the TPP python isobarQuant package (available from GitHub at <https://github.com/protcode/isob>, Python 2.7 was used) and the TPP R package available

from Bioconductor (<http://bioconductor.org/packages/TPP/>). Data were first extracted using the python package with the preMascot.py command. TMT isotope interference was indicated in the QuantMethod configuration file prior to this step. The FASTA database for *Mus musculus* was downloaded (16,985 Swiss-Prot entries accessed on July 25, 2018), and a new FASTA file containing both forward and reverse (decoy) sequences was created according to their instructions. Mgf files created from preMascot workflow were searched against the combined database using Mascot Daemon with the following parameters: cysteine carbamidomethylation and TMT (lysine) as fixed modifications, methionine oxidation and TMT (N-term) as variable modifications, max. 2 tryptic missed cleavages, peptide tolerance of 10 ppm (Mascot version 2.5.1, Matrix Science). The searched results (.dat files) were further processed in the postMascot workflow. In this step, peptides and proteins were filtered based on a set of criteria such as FDR threshold. One good quality peptide was sufficient to infer protein identification. Peptide quantification values are corrected for interference caused by co-eluting precursors contributing to TMT signal using signal to interference (S2I) ratios.^[78] Finally, results from 8 high pH fractions were merged to generate protein level summaries for each experiment condition (e.g. control, drug treatment). The protein text files are then processed using analyzeTPPTR function in TPP R package (version 3.6.0) to generate melting curves based on fold changes and to identify statistically significant shifts. Analysis of the TPP TR melting curves was described in the Introduction.

4.3.2 PISA TPP experiment

Cell Culture and Lysis

TIL1 cells were harvested and lysed the same way as the conventional TPP method described above. The cell lysate was diluted with more lysis buffer to a final concentration of ~2mg/ml and then divided into aliquots. For lysate #1 and #2, lysates were split into 3 aliquots of 247.5 μ l each and each aliquot was treated with 2.5 μ l of DMSO, 2.5 μ l of 0.1 mM Compound 512 (1 μ M final concentration) or 2.5 μ l of 1mM Compound 512 (10 μ M final concentration). For lysate #3, lysate was divided to 4 aliquots of 247.5 μ l each and the aliquot was treated with 2.5 μ l of DMSO, 0.01 mM 512 (0.1 μ M final concentration), 0.1 mM 512 (1 μ M final concentration), or 1 mM 512 (10 μ M final concentration). After gentle mixing of each tube, they were incubated at room temperature for 30 min.

Drug Incubation and Heat Treatment

After drug incubation, the lysates were further divided into 10 PCR tubes of 20 μ l aliquots. These 20 aliquots were heated for 3 min on a PCR machine with a temperature gradient setup (37, 41, 44, 47, 50, 53, 56, 59, 63, 67 $^{\circ}$ C), followed by a cool down at 4 $^{\circ}$ C for 3 min. The heated cell lysates were pooled into 150 μ l samples and were ultracentrifuged at 100,000 g (48,000 RPM for TLA 100 rotor on a Beckman Coulter ultracentrifuge) for 20 min at 4 $^{\circ}$ C. After centrifugation, 130 μ l supernatants were collected without touching the pellet. Protein concentration of each sample was determined by the BCA assay.

MS Sample Preparation

Proteins were precipitated by adding 4X volumes of cold acetone (480 μ l) and cooled for 2 hours at -20 $^{\circ}$ C. The supernatants were removed by vacuum centrifugation at 8000 g for 15 min. When the acetone was mostly evaporated, the pellet was

resuspended in 200 μ l membrane compatible buffer containing 50mM triethylammonium bicarbonate (TEAB) with 0.5% sodium deoxycholate, and 12 mM sodium lauryl sarcosine. The proteins were denatured by sonication for 5 min, followed with heating at 95°C for 5 min. Disulfide bonds were reduced by tris(2-carboxyethyl)phosphine (TCEP) at room temperature for 30 min (5 mM final concentration). Cysteine residues were alkylated by iodoacetamide (12.5 mM final concentration) at room temperature in the dark for 30 min. The sample was diluted 5 fold with 50 mM TEAB. Proteins were digested by MS Grade trypsin with a 1:50 enzyme: protein ratio and incubated at 37°C overnight.

Peptides were acidified with trifluoroacetic acid (TFA) to a final concentration of 0.5% and vortexed for 5 min. To each sample, ethyl acetate (1:1 v/v) was added for detergent removal and vortexed for 5 min. The mixture was centrifuged at 12,000 g for 10 min, and the upper organic phase was removed. The ethyl acetate extraction was repeated once. Samples were desalted with C18 Micro spin columns (17-170 μ g capacity, Nest Group). Peptide concentration from each sample was determined by fluorescent peptide quantitation assay (Pierce).

For TMT labeling, peptide samples were resuspended in 100 μ l 200mM HEPES, 30% ACN. To each TMT-10 plex label, 41 μ l ACN was added to dissolve the tags for 5 min with occasional vortexing. The labeling reaction went on for one hour and was quenched with 8 μ l 5% hydroxylamine (in 200 mM HEPES) for 15 min, followed by acidification to 5% formic acid. The 10 samples from all 3 biological replicates were combined. The pooled sample was desalted with Pierce Peptide Desalting column before MS analysis.

Liquid Chromatography–Mass Spectrometry

This TMT10 sample was dried and resuspended in 200 μ l 0.1% formic acid/3% ACN, and 1 μ l was injected into a 15 cm by 75 μ m nanoViper C18 column (Thermo). A 150-minute water-acetonitrile gradient was applied on a Dionex Ultimate 3000 UHPLC system (Thermo Fisher Scientific) at a flow rate of 300 nl/min: at 10 min, 0% B; at 11-16 min, ramp to 7% B; from 16 to 116 min, ramp to 25% B; from 116 to 136 min, ramp to 60% B; by 137 min, ramp to 95% B; hold at 95% B till 142 min; 143-150 min, equilibrate to 3% B (Buffer A: water with 0.1% formic acid and Buffer B: acetonitrile with 0.1% formic acid). Peptides were ionized and introduced into the QE plus mass spectrometer (Thermo Fisher Scientific).

All MS1 spectra were acquired over m/z 350–1400 in the Orbitrap (70 K resolution at 200 m/z); automatic gain control (AGC) was set to accumulate 3E6 ions, with a maximum injection time of 50 ms. Top 15 data-dependent MS/MS analysis was performed using HCD in the Orbitrap. The normalized collision energy was optimized at 30% for HCD. Isolation window was 1.2 m/z . MS2 spectra were acquired with resolution of 35 K and a fixed first m/z of 100. The intensity threshold for fragmentation was set to 10000, and included charge states 2+ to 7+. A dynamic exclusion of 30 s was applied.

Data Analysis

Data analysis was performed with Thermo Proteome Discoverer 2.2 using workflows recommended by Thermo for a TMT experiment using the QE type of instruments. Data was searched against the Uniprot *Mus musculus* database using Sequest HT with TMT6plex (+229.163) and methionine oxidation as dynamic modifications and carbamidomethyl as static modification. Data was validated by Percolator. For reporter ion quantification, an isotope impurity correction was applied. A

co-isolation threshold was set to 50 and an average reporter S/N threshold was 10. Intensities were normalized to total peptide amount in each channel so that all TMT channels have the same total abundance. The data was analyzed twice with the same settings but with a different study design. In one study, individual TMT channels were kept as separate abundances, and ratios of each compound-treated channel to their corresponding control channel within the same biological replicate set were computed. In the other analysis, I used a grouped study design, whereby all samples pertaining to the same drug concentrations were combined into a summed abundance and ANOVA p-values for each group comparison could be obtained.

4.4 Results and Discussion

4.4.1 Results from conventional TPP experiment

Analysis of two sets of biological replicates using the TPP R package (Table 4.1) returned a total of 7322 proteins with thermal stability data. Among these proteins, 3720 (bio rep 1) or 3932 (bio rep 2) proteins passed the melting curve filters (e.g. plateau <0.3 and $R^2>0.8$) and were used for p-value calculation. As we can see from here, the curve fitting filter criteria are quite stringent and about half of the proteins were not considered for differential statistical analysis. Eventually, 12 proteins passed the final 4 criteria for significant shifts as described previously, and these are the proposed targets from this TPP experiment (Table 4.2). Half of the 12 proteins showed stabilization by the compound 512, whereas the other half presented destabilization.

Table 4.1: TPP experiment configuration table in TPP R package. 1 & 2 indicates two biological replicates. 126-131L denotes TMT labels and corresponding temperature treatments.

Experiment	Condition	Comparison1	Comparison2	126	127L	127H	128L	128H	129L	129H	130L	130H	131L
Vehicle_1	Vehicle	x		67	63	59	56	53	50	47	43	41	37
Vehicle_2	Vehicle		x	67	63	59	56	53	50	47	43	41	37
512_1	Treatment	x		67	63	59	56	53	50	47	43	41	37
512_2	Treatment		x	67	63	59	56	53	50	47	43	41	37

Table 4.2: Proteins with significant melting curve shifts between control and the 512-treated lysates. Blue shaded proteins were stabilized by 512 (right shift in melting curve) and yellow shaded proteins were destabilized by 512 (left shift in melting curve).

Gene	Protein	Biological function	Cellular localization
TUSC2	Tumor suppressor candidate 2 (Fus1 protein)	Regulation of mitochondrial homeostasis	Mitochondria
H1F0	Histone H1.0	Chromatin condensation	Nucleus
SKAP1	Src kinase-associated phosphoprotein 1	Positive regulation of immune response	Plasma membrane, cytosol, nucleus
MCCC1	Methylcrotonoyl-CoA carboxylase subunit alpha	Leucine catabolic process	Mitochondria
CHM	Rab proteins geranylgeranyltransferase component A 1	Rab GTPase binding	Cytosol
MRPL17	39S ribosomal protein L17	Translation	Mitochondria
RIPK3	Receptor-interacting serine/threonine-protein kinase 3	Necroptosis, programmed cell death process in response TNF-alpha	Cytosol, membrane, mitochondria
SDHC	Succinate dehydrogenase cytochrome b560 subunit, mitochondrial	TCA, mitochondrial electron transport	Mitochondria
NIP7	60S ribosome subunit biogenesis protein NIP7 homolog	Ribosome assembly	Nucleus
FNTB	Protein farnesyltransferase subunit beta	Response to organic cyclic compound; regulation of cell proliferation	Cytoskeleton
TAPT1	Transmembrane anterior posterior transformation protein 1	Cartilage and bone development	Cytoskeleton
LSM12	Protein LSM12 homolog	RNA metabolic process	

When we take a closer look at the melting curves for the 6 stabilized proteins in Figure 4.10, we see that not every proposed target is equally believable although they all passed the filters and significance tests. The top 3 proteins in this figure has more consistent melting curve profiles between the two biological replicates, whereas the bottom 3 proteins showed some anomaly in their melting curve trend that made their results appear less reliable. Based on this result, I performed protein network analysis and further functional investigations focusing on the top 3 protein targets: TUSC2, SKAP1, and H1F0.

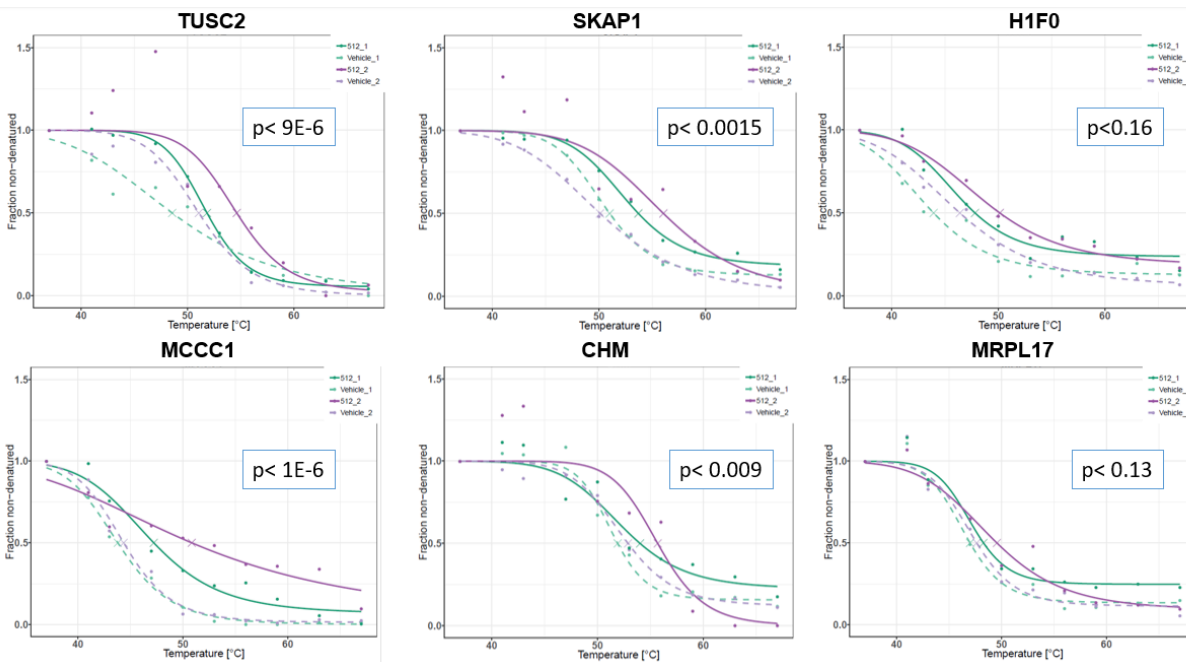


Figure 4.10: Melting curves of the 6 proteins that were stabilized by 512. Y-axis is normalized protein abundance fold change relative to lowest temperature (i.e. 37°C). Dotted line is control and solid line is drug treated sample. Green and purple are two biological replicates. P-value here is taken from one of the two biological replicate comparisons.

As an initial analysis of the 12 protein targets, I mapped the relationship between these proteins using String network analysis tool (Figure 4.11). Besides these 12 proteins as input, I added additional interactors that might help with mapping out the associations (e.g. Ptprc, Cdk2). String presents a map of protein-protein associations collected from experimental data, computational prediction, as well as co-mentioning in literature. Some connections start to emerge between the targets, particularly between Skap1 and Histone H1. Interestingly, both SKAP1 and histone H1 participate in signaling pathways that promote cell proliferation. They are connected through Cdk2, which is a key regulator of DNA damage-activated G1-S phase checkpoints.^[79]

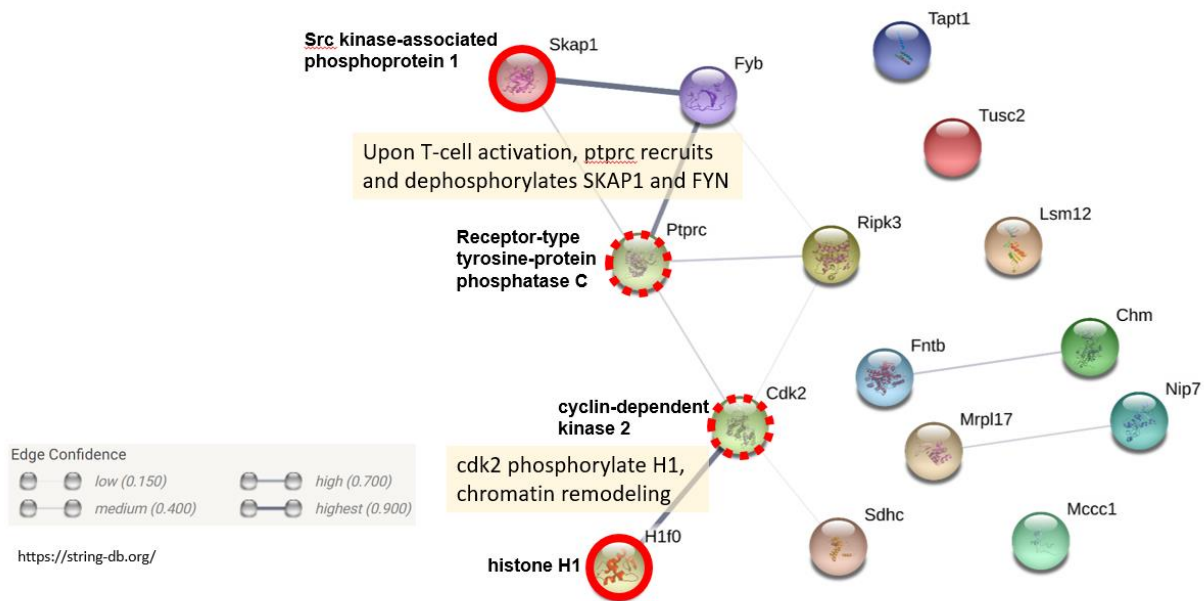


Figure 4.11: String Functional Protein Association Network analysis. A thicker line of connection indicates higher confidence of association. Skap1 and H1f0 are actual targets from my experiment (indicated as solid red circles); Ptprc and Cdk2 were artificially added as interactors (indicated as dotted red circles).

These two proteins are both plausible targets for the radiation mitigation drug because of their involvement in T cell activation and DNA damage response. Specifically, SKAP1 is involved in T cell activation and generates adaptive immune response. After ionizing radiation, T cell activation is impaired and T cells are highly sensitive to radiation-induced injury (they undergo interphase apoptotic death within hours after irradiation).^[80] CDK levels are normally low in resting T cells, but are increased in G1 phase after upon T cell receptor stimulation. Cdk2 is able to phosphorylate Histone H1, which then relaxes chromatin structure, and allows the DNA repair complexes to access the site of damage (Figure 4.12).^[81] Based on this connection between Skap1 and Histone H1, my first hypothesis for a mechanism of action is that compound 512 rescues T cell activation and stimulates cell proliferation and immune response through a DNA damage response pathway.

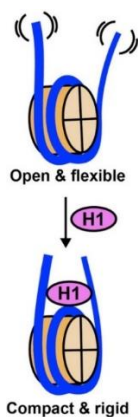


Figure 4.12: Histone H1 compacts chromatin structure.^[82]

Tumor suppressor protein (TUSC2 or Fus1 protein) is another plausible target for a radiomitigator. Studies have demonstrated the radioprotective function of this protein through maintaining balanced ROS production and mitochondrial homeostasis.^[83,84] In the first experiment, Fus1-deficient mice were found to suffer from higher radiosensitivity manifested in compromised crypt generation in GI tract, and other tissues (Figure 4.13).^[84] This radiosensitivity was later found to be caused by dysregulation of antioxidant response by the follow-up experiment.^[83] Treatment with inhibitor of pathogenic oxidative reactions, pyridoxamine (PM) significantly ameliorated IR-induced damage to the GI epithelium in Fus1 KO mice and significantly enhanced survival of irradiated mice (Figure 4.13).^[83] Their experiments also showed that Fus1 KO cells had higher levels of ROS and chronic oxidative stress. This is congruent with the fact that mitochondria are a major source of ROS following IR leading to chronic injury of the cell (Figure 4.14).^[85] This forms the basis of my second hypothesis for Compound 512's mechanism, which is that 512 targets Fus1 to activate antioxidant response pathways to provide radiation mitigation.

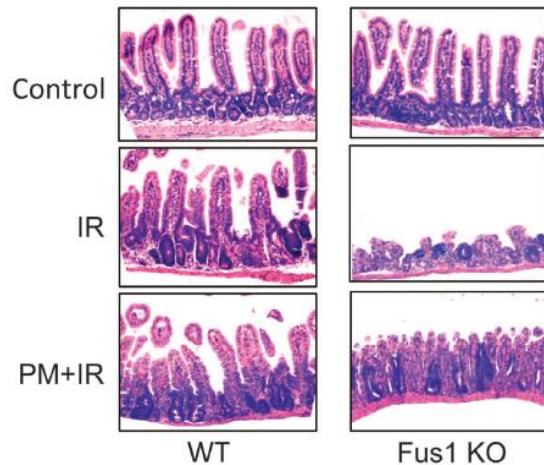


Figure 4.13: Morphology of intestinal crypts of wild type and Fus1 KO mice treated to 12 Gy whole body ionizing radiation (IR). Last panel is mice treated with PM or pyridoxamine, inhibitor of pathogenic oxidative reactions.^[83]

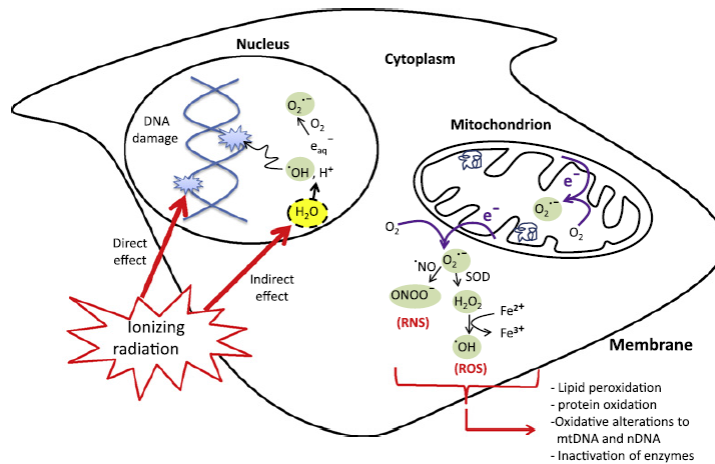


Figure 4.14: IR induces metabolic oxidative stress from generation of RNS and ROS in mitochondria besides direct DNA damage.^[85]

4.4.2 Results from PISA TPP experiment

The original goal to perform additional TPP experiment using the PISA approach is to validate the 12 targets I found from the conventional TPP experiment, and discover additional hypothetical targets that might be previously eliminated in the stringent curve fitting procedure. However, data analysis for PISA experiment is not as straightforward as I expected, since PISA is a new methodology and only a proof-of-principle has been described in the bioRxiv article.^[77] In my opinion, many more iterations of this type of

experiments have to be performed to optimize the experiment protocol, experimental design and data processing procedure. Here in this early work, I evaluate the performance of the instrument and data quality, propose some hypothetical targets based on preliminary thresholds, and describe some considerations and challenges associated with data analysis.

To make full use of the TMT10 reagent set, I performed a triplicate of the 2D PISA experiment as show in Table 4.3, in which two sets of biological replicates (1,2) were treated with two drug concentrations (1 μ M and 10 μ M), and last set of biological replicates (3) were treated with three concentrations (0.1 μ M, 1 μ M and 10 μ M). This experimental design is similar to the proposed scheme in the PISA article (Figure 4.9, h). Data was acquired on a QE plus platform and analyzed using Thermo Proteome Discoverer software version 2.2 (PD 2.2).

Table 4.3: TMT10 labeling scheme for PISA experiment.

TMT126	TMT127 N	TMT127 C	TMT128 N	TMT128 C	TMT129 N	TMT129C	TMT130N	TMT130C	TMT131
Bio Rep 1 Control	Bio Rep 1 512 (1uM)	Bio Rep 1 512 (10uM)	Bio Rep 2 Control	Bio Rep 2 512 (1uM)	Bio Rep 2 512 (10uM)	Bio Rep 3 Control	Bio Rep 3 512 (0.1uM)	Bio Rep 3 512 (1uM)	Bio Rep 3 512 (10uM)

A total of 1951 proteins was identified with high FDR confidence, which is slightly lower than the number of proteins identified in unlabeled samples on the same platform (range from 2323 to 2794). To look into this issue of relatively low protein ID's in the TMT run, I compared precursor intensity and ion injection time between this TMT run and a control sample just prior to TMT labeling. From the PD distribution charts, the TMT run had a greater proportion of precursor ions with the lowest intensity level (Figure 4.15). At the MS/MS level, the TMT run also had a greater proportion of MS2 ions with maximum (100 ms) ion injection time (Figure 4.16). These factors suggest not enough ions were accumulated and there is room for improvement in fine-tuning instrument parameters to

increase peptide and protein ID, despite using Thermo's recommended settings for a TMT10 experiment on a QE plus.

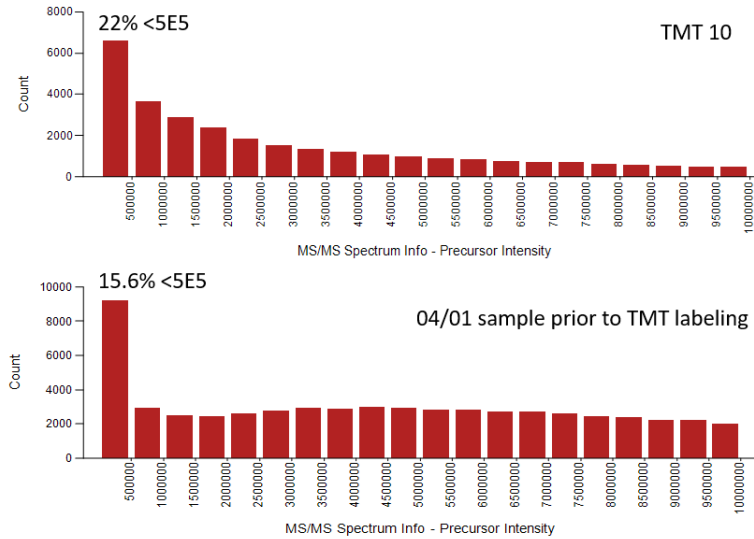


Figure 4.15: Precursor intensity for TMT 10 labeled sample vs. a control sample prior to TMT labeling analyzed on the QE plus.

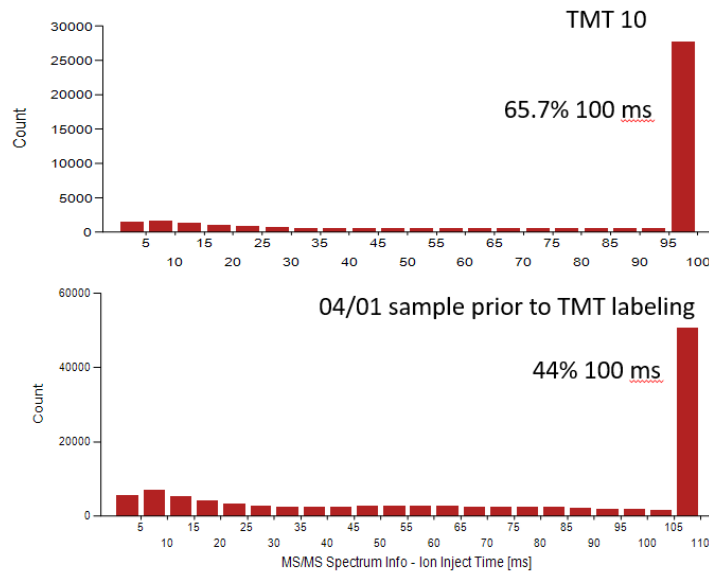


Figure 4.16: Ion injection time for TMT 10 labeled sample vs. a control sample prior to TMT labeling analyzed on the QE plus.

In terms of quantitative accuracy, precursor isolation interference is an important factor. For the QE instrument, quadrupole isolation window is typically set to 1.6-2 m/z.

The QE plus is equipped with Advanced Quadrupole Technology (AQT) that allows more efficient ion transmission at narrower isolation width, therefore a narrower window such as 0.7 or 1.2 m/z can be selected to reduce number of interference ions that are co-isolated with the precursor ions in order to improve the reporter ion quantification accuracy. In my PISA TMT run on the QE plus, a 1.2 m/z isolation window was selected. If we examine the percentages of isolation interferences and compare the different isolation windows from the QE, QE plus and Fusion Lumos, we can see that the narrowest isolation window on the Lumos yield TMT MS2 data with the least isolation interference and best quantitative accuracy (Figure 4.17). In my PD data processing, a default threshold of 50% isolation interference was set to eliminate reporter ions with high co-isolations. Beyond isolation window and ion injection time, all critical instrument parameters (resolution, AGC target, collision energy, etc.) have to be carefully selected and further optimized to achieve best sensitivity and quantitative accuracy for a TMT 10 experiment.

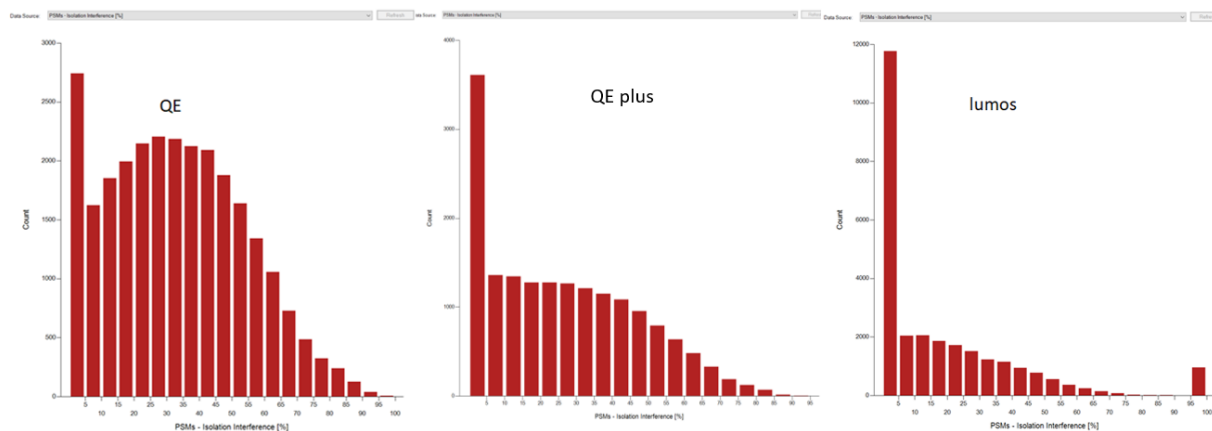


Figure 4.17: Isolation interference of TMT 10 experiment acquired with 1.6 m/z isolation window on a QE, with 1.2 m/z isolation on a QE plus, and 0.7 m/z isolation on a Fusion Lumos.

Ideally what we expect to see from this set of PISA TPP experiments is increased summed protein abundance in compound-treated sample compared to control for potential targets across all replicates, and also increased response for higher compound concentrations (higher abundance in 10 uM compared to 1 uM 512). Based on this premise, the most stringent criteria for finding candidate targets would be a significant fold change for each of the compound-treated and control pair, that is consistent across 3 sets of biological replicates. Furthermore, the fold changes should be concentration dependent with the strongest differential expression in samples treated with the highest compound concentration. In practice, when I subject the data with $FC > 1$ cutoff for each pair of comparison (abundance ratio of each compound-treated channel to corresponding control channel), only 40 proteins survived. Unfortunately, none of them seem to display consistent trends for fold changes across the 3 biological replicates, nor do they display consistent behavior for concentration dependency (Figure 4.18).

Peptide Groups	PSM	MS/MS Spectrum Info	Quan Spectra	Input Files	Specialized Traces	Accession	Description	Coverage (%)	Sequence Coverage	# Peptides	# PSM	# Unique Peptides	# AA	MW (kDa)	calc. pI	Score Sequ	# Peptides i	# Razor Peptides	Abundance Ratios							
						P59017	Bcl-2-like protein 13 OS-Mus musculus OX-10090 GN-HdD11	3%		1	1	1	434	46.7	4.59	2.27	1	0	(127N) / (126)	(127C) / (126N)	(128N) / (128N)	(129N) / (128N)	(130N) / (129C)	(130C) / (129C)	(131) / (121) / (11)	1.692
						P12265	Beta-glucuronidase OS-Mus musculus OX-10090 GN-HdG F	1%		1	2	1	648	74.1	6.70	0.00	1	0	0	1.151	1.196	1.182	1.033	1.459	1.032	1.692
						OC3280	Serine/threonine-protein kinase CNK1 OS-Mus musculus OX-1	3%		1	1	1	476	54.3	8.18	2.51	1	0	0	1.772	1.657	1.285	1.198	1.349	1.222	1.534
						Q9VFE0	Ribulose-1,5-bisphosphate 3-epimerase OS-Mus musculus OX-10090	25%		4	5	4	228	24.9	5.41	11.60	4	0	0	1.033	1.060	1.028	1.029	1.054	1.037	1.166
						Q8R4W6	Eukaryotic translation initiation factor 2A OS-Mus musculus OX-	13%		4	4	4	581	64.4	8.91	8.85	4	0	0	1.067	1.009	1.035	1.072	1.064	1.030	1.148
						Q8R9C4	WD repeat-containing protein 82 OS-Mus musculus OX-10090	4%		1	1	1	313	35.1	7.69	3.61	1	0	0	1.122	1.059	1.099	1.225	1.188	1.247	1.111
						Q8C402	SRP and G-protein domain-containing protein 1 OS-Mus muscu	2%		1	1	1	643	72.6	7.64	1.85	1	0	0	1.152	1.067	1.110	1.130	1.228	1.303	1.105
						Q9WV91	Prostaglandin F2 receptor negative regulator OS-Mus muscu	2%		1	1	1	879	98.7	6.61	2.75	1	0	0	1.068	1.104	1.345	1.222	1.045	1.345	1.103
						P54923	Protein ADP-ribosyltransferase OS-Mus musculus OX-	5%		1	1	1	352	40.0	5.75	2.73	1	0	0	1.203	1.105	1.223	1.077	1.059	1.062	1.091
						P62301	40S ribosomal protein S13 OS-Mus musculus OX-10090 GN-H-	8%		1	1	1	151	17.2	10.54	2.23	1	0	0	1.267	1.009	1.117	1.219	1.026	1.084	1.087
						Q00612	Glucose 6-phosphate 1-dehydrogenase X OS-Mus musculus C	17%		8	12	8	515	59.2	6.49	31.71	8	0	0	1.012	1.010	1.020	1.028	1.026	1.074	1.078
						P29341	Polysialyltransferase 1 OS-Mus musculus OX-10090	21%		12	14	12	636	70.6	9.50	37.15	12	0	0	1.081	1.006	1.035	1.046	1.034	1.044	1.077
						Q9Q793	ACTP pyrophosphatase 1 OS-Mus musculus OX-10090 GN-H-	26%		3	3	3	170	18.8	5.03	11.87	3	0	0	1.073	1.031	1.020	1.041	1.013	1.067	1.073
						P14576	Signal recognition particle 54 kDa protein OS-Mus musculus O	20%		7	7	7	504	55.7	8.75	21.65	7	0	0	1.093	1.022	1.079	1.001	1.006	1.084	1.067
						P62075	Mitochondrial import inner membrane translocase subunit Tim1	26%		2	4	2	95	10.5	8.18	16.31	2	0	0	1.155	1.120	1.062	1.079	1.027	1.059	1.067
						P62293	Importin subunit alpha 1 OS-Mus musculus OX-10090 GN-H-C	17%		6	9	6	529	57.9	5.68	23.89	6	0	0	1.048	1.010	1.018	1.015	1.031	1.024	1.060
						Q8C0N6	Theodoxon-like protein 1 OS-Mus musculus OX-10090 GN-H+	38%		7	12	7	289	32.2	4.96	44.25	7	0	0	1.072	1.074	1.016	1.011	1.031	1.031	1.068
						P47963	60S ribosomal protein L13 OS-Mus musculus OX-10090 GN-H-	13%		4	5	4	211	24.3	11.55	10.39	4	0	0	1.192	1.061	1.013	1.062	1.027	1.034	1.041
						P83372	Tubulin beta-48 chain OS-Mus musculus OX-10090 GN-H-HdK	71%		24	90	4	445	49.8	4.89	285.75	24	0	0	1.014	1.009	1.024	1.033	1.057	1.078	1.039
						P84899	60S ribosomal protein L19 OS-Mus musculus OX-10090 GN-H-	22%		4	4	4	196	23.5	11.47	7.15	4	0	0	1.057	1.060	1.085	1.144	1.021	1.061	1.038
						Q9C926	40S ribosomal protein S19 OS-Mus musculus OX-10090 GN-H-	47%		9	16	9	145	16.1	10.40	45.54	9	0	0	1.014	1.007	1.033	1.027	1.034	1.031	1.037
						P24547	Inosine 5'-monophosphatase dehydrogenase 2 OS-Mus muscu	44%		19	32	17	514	55.8	7.28	118.72	19	2	0	1.022	1.040	1.004	1.027	1.004	1.027	1.034
						Q9J462	Replication factor C subunit 4 OS-Mus musculus OX-10090 G	6%		2	2	2	364	39.6	6.70	3.38	2	0	0	1.087	1.031	1.023	1.034	1.010	1.018	1.034
						Q71K60	Heterogeneous nuclear ribonucleoprotein Q OS-Mus muscu	7%		8	13	8	623	69.6	8.59	36.01	8	0	0	1.121	1.061	1.070	1.117	1.044	1.017	1.033
						Q53207	Cyclin-dependent kinase 2 associated protein 1 OS-Mus musc	15%		1	1	1	114	12.3	9.48	2.89	1	0	0	1.042	1.020	1.297	1.068	1.015	1.115	1.032
						Q8C9Y4	Cyclin-dependent kinase 2 associated protein 2 OS-Mus musc	6%		1	1	1	127	13.2	9.48	2.89	1	0	0	1.042	1.020	1.297	1.068	1.015	1.115	1.032
						P62245	40S ribosomal protein S15a OS-Mus musculus OX-10090 GN	53%		7	7	7	130	14.8	10.13	16.33	7	0	0	1.111	1.022	1.038	1.080	1.013	1.033	1.030
						P61161	Actin-related protein 2 OS-Mus musculus OX-10090 GN-HdK	25%		9	11	8	394	44.7	6.74	35.73	9	0	0	1.032	1.015	1.013	1.001	1.010	1.005	1.027
						Q9J415	DNAZ-associated protein 1 OS-Mus musculus OX-10090 GN-H-	10%		3	4	3	432	43.2	9.27	3.3	3	0	0	1.107	1.043	1.050	1.029	1.035	1.078	1.026
						Q8C9T8	Zinc finger protein Helix OS-Mus musculus OX-10090 GN-HdK	2%		1	1	1	526	59.4	8.06	0.00	1	0	0	1.139	1.077	1.066	1.023	1.123	1.106	1.022
						Q8C9W3	Zinc finger protein Helix OS-Mus musculus OX-10090 GN-HdK	2%		1	1	1	892	101.7	8.09	0.00	1	0	0	1.139	1.077	1.066	1.023	1.123	1.106	1.022
						P66648	60S ribosomal protein L10 OS-Mus musculus OX-10090 GN-H-	13%		4	6	4	214	24.6	10.08	9.77	4	0	0	1.145	1.040	1.027	1.079	1.027	1.010	1.020
						P14131	40S ribosomal protein S16 OS-Mus musculus OX-10090 GN-H-	23%		3	3	3	146	16.4	10.21	8.91	3	0	0	1.199	1.018	1.036	1.125	1.039	1.004	1.013
						P62639	Tat1 OS-Mus musculus OX-10090 GN-HdK PFC+ SV+2	37%		56	67	48	2541	269.7	6.18	213.91	56	4	0	1.040	1.023	1.015	1.005	1.013	1.004	1.007
						P62309	Small nuclear ribonucleoprotein G OS-Mus musculus OX-100	31%		5	8	5	76	8.5	8.88	16.84	5	0	0	1.032	1.046	1.051	1.005	1.019	1.042	1.000
						Q8C9C7	Phenylalanine-tRNA ligase alpha subunit OS-Mus musculus C	7%		3	3	3	508	57.6	8.28	6.25	3	0	0	1.043	1.021	1.078	1.040	1.059	1.047	1.000

Figure 4.18: Thermo PD display of proteins that have increased abundance in compound treated sample compared to control sample in every pair of comparison across the biological replicates and compound concentrations. Abundance ratios of each compound-treated channel vs. control channel are shown on the right side of the table.

To better filter for candidates with more suitable significance threshold, I re-did the analysis on the Thermo PD with a grouped experimental design, in which all the replicates with the same drug concentrations (DMSO, 0.1 μ M, 1 μ M, 10 μ M) were grouped together into an averaged abundance as shown in Figure 4.19 and ratios for these grouped abundances were computed along with the ANOVA p-values. From this dataset, I generated volcano plots to visualize proteins with significant fold changes. Typically, a p-value of 0.01 or 0.05 is applied for differential abundance. Here I decided to use a more relaxed p-value threshold of 0.1 to capture more potential targets in this early stage. For the fold change, I decided to use a cutoff of 1.2 based on the histogram distribution of fold changes. With these relaxed thresholds, only 5 proteins passed my criteria (Figure 4.20). It is also surprising to see that the lower concentration yielded more significant changes, since we expect 10 μ M to be the saturating compound concentration that causes a more pronounced effect.

Sample	Sample Identifier	Sample Type	drug concentration
<input type="checkbox"/>	<input type="checkbox"/> TMT10	<input type="checkbox"/>	<input type="checkbox"/>
<input type="checkbox"/> S13	20190827_PISA_TMT10_1uM_NCE30 - [126]	Control	DMSO
<input type="checkbox"/> S19	20190827_PISA_TMT10_1uM_NCE30 - [127N]	Sample	1uM
<input type="checkbox"/> S20	20190827_PISA_TMT10_1uM_NCE30 - [127C]	Sample	10uM
<input type="checkbox"/> S21	20190827_PISA_TMT10_1uM_NCE30 - [128N]	Control	DMSO
<input type="checkbox"/> S22	20190827_PISA_TMT10_1uM_NCE30 - [128C]	Sample	1uM
<input type="checkbox"/> S23	20190827_PISA_TMT10_1uM_NCE30 - [129N]	Sample	10uM
<input type="checkbox"/> S24	20190827_PISA_TMT10_1uM_NCE30 - [129C]	Control	DMSO
<input type="checkbox"/> S25	20190827_PISA_TMT10_1uM_NCE30 - [130N]	Sample	0p1uM
<input type="checkbox"/> S26	20190827_PISA_TMT10_1uM_NCE30 - [130C]	Sample	1uM
<input type="checkbox"/> S27	20190827_PISA_TMT10_1uM_NCE30 - [131]	Sample	10uM

Figure 4.19: Grouped study design in Thermo PD. Each channel is labeled with the corresponding type of drug concentration, so that the same drug concentrations are combined into group abundances and p-value could be computed.



Figure 4.20: Volcano plots from Thermo PD that shows differential grouped abundances comparing 10 uM or 1 uM to DMSO. The red and green shaded areas indicate significant fold change and p-value. Proteins that pass threshold are labeled with their names.

Upon closer inspection of the quality of MS data for these 5 proteins, not all of them have the same level of confidence in identification and quantification (Table 4.4). For example, the top 3 proteins in this table had quite low reporter ion intensities, which are close to the reporter ion S/N threshold of 10 set in the analysis. Also, proteins in rows 2 and 3 had only 1 PSM for identification, making these results less trustworthy.

Table 4.4: Protein level summary from Thermo PD for the 5 proteins that showed significant fold changes in Volcano plots. The upper table shows grouped abundance results; the lower table shows individual abundances from all TMT channels.

Accession	Description	Coverage	# Peptide	# PSMs	# Unique Peptides	# Peptide (DMSO)	Abundance Ratio: (0p1uM) / (DMSO)	Abundance Ratio: (1uM) / (DMSO)	Abundance Ratio: (10uM) / (DMSO)	Abundance Ratio P-Value: (0p1uM) / (DMSO)	Abundance Ratio P-Value: (1uM) / (DMSO)	Abundance Ratio P-Value: (10uM) / (DMSO)
P12265	Beta-glucuronidase	1	1	2	1	1	1.349	1.74	1.628	0.00986259	0.024674374	
Q91WG2	Rab GTPase-binding effector protein 2	2	1	1	1	1	0.691	1.346	1.039	0.05013193	0.501346477	
Q8VE88	Protein FAM114A2	2	1	1	1	1	0.897	1.44	1.337	0.0510534	0.33214671	
Q3UDE2	Tubulin--tyrosine ligase-like protein 12	13	6	6	6	6	1.094	1.62	1.105	0.08197686	0.667751942	
P61202	COP9 signalosome complex subunit 2	7	3	4	3	3	0.888	1.226	1.117	0.09859094	0.230806798	

Accession	Description	Abundance: F3: 126, Control, DMSO	Abundance: F3: 128N, Control, DMSO	Abundance: F3: 129C, Control, DMSO	Abundance: F3: 127N, Sample, 1uM	Abundance: F3: 128C, Sample, 1uM	Abundance: F3: 130C, Sample, 1uM	Abundance: F3: 127C, Sample, 10uM	Abundance: F3: 129N, Sample, 10uM	Abundance: F3: 131, Sample, 10uM	Abundance: F3: 130N, Sample, 0p1uM
P12265	Beta-glucuronidase	7.8	9.2	9	14.1	13.7	13.1	13.1	13.5	13.5	11
Q91WG2	Rab GTPase-binding effector protein 2	18.3	14.8	15.7	26.2	22.9	18.6	19	17.4	22.6	12.7
Q8VE88	Protein FAM114A2	10.6	10.8	13.7	19.2	16.5	15.2	16.8	11.2	18	11.1
Q3UDE2	Tubulin--tyrosine ligase-like protein 12	120.2	79	115	179	156	110.2	113.9	109.5	148.9	113.9
P61202	COP9 signalosome complex subunit 2	50	39.4	51.1	60.1	57.3	46.2	54.4	52.9	59.3	43.6

From examining the data, it seems that we need additional QC metrics that are more stringent than the default recommended settings for a TMT experiment in Thermo PD to filter out poor quality proteins. In my opinion, these metrics can be established based on repeated analysis of the sample to see at which level of cutoff the filters can generate reproducible protein level results. Some key metrics to consider are:

- (1) Reporter ion signal to noise ratio
- (2) Isolation interference %
- (3) Precursor ion intensity
- (4) # peptide spectral matches
- (5) # unique peptides per protein

Lastly, I compared the hypothetical targets found in conventional TPP experiment to the PISA experiment results. I searched the 12 protein accessions in this PISA dataset and found only 2 of the 12 proteins were also identified here (Table 4.5), and only 1 protein had quantification values. Considering the PISA experiment was done using the same lysates as the conventional replicates, I would expect more overlap in the result. In reality, these two datasets seemed to have a lot of differences in which proteins were identified and whether their abundances went up or down upon compound treatment.

Table 4.5: Previously identified targets that were also found in the PISA data.

Accession	Description	Coverage [%]	# Peptides	# PSMs	# Unique Peptides	# AAs	MW [kDa]	calc. pI	HT	Score Sequest HT: Sequest	# Peptides (by Search Engine): Sequest	# Razor Peptides	Abundance Ratio: (127N) / (126)	Abundance Ratio: (127C) / (126)	Abundance Ratio: (128C) / (128N)	Abundance Ratio: (129N) / (128N)	Abundance Ratio: (130N) / (129C)	Abundance Ratio: (130C) / (129C)	Abundance Ratio: (131) / (129C)
Q9D0R8	Protein LSM12 homolog	14	3	4	3	195	21.7	7.74	11.16	3	0	0.976	1.037	1.01	1.029	0.952	1.037	0.994	
Q9CZ80	Succinate dehydrogenase cytochrome	5	1	1	1	169	18.4	9.94	2.2	1	0								

4.5 Conclusion

From the early stage of testing TPP protocols, reproducibility has been a concern. For the conventional TPP experiment, the protocol that I created has additional steps to

solubilize membrane proteins and subsequent detergent removal. It is possible that these additional steps introduce more sources of variability between replicate experiments, and a very simplified and automated workflow is needed to achieve reproducible results. The PISA approach is more simplified since all temperature points are pooled together for downstream sample preparation. The main concern here is that the selection of which temperature points we choose to combine will affect the extent of the fold changes of the targets. Ideally, we would only want to pool the temperatures that generate the biggest differences between control and drug-treatment (close to melting point); however, in a discovery stage, we don't know the targets or their melting points in advance. In this first PISA experiment, all temperatures from 37 to 67 °C were combined. Perhaps a better temperature range is somewhere in between. As the community starts to adopt and perform more TPP experiments for target identification, more standard practices will be established.

REFERENCES

- [1] J. P. Williams, W. H. McBride, *Int. J. Radiat. Biol.* **2011**, *87*, 851.
- [2] C. I. Rios, D. R. Cassatt, A. L. DiCarlo, F. Macchiarini, N. Ramakrishnan, M.-K. Norman, B. W. Maidment, *Drug Dev. Res.* **2014**, *75*, 23.
- [3] V. K. Singh, V. L. Newman, P. L. Romaine, M. Hauer-Jensen, H. B. Pollard, *Expert Rev. Mol. Diagn.* **2016**, *16*, 65.
- [4] C. A. Crutchfield, S. N. Thomas, L. J. Sokoll, D. W. Chan, *Clin. Proteomics* **2016**, *13*, 1.
- [5] K. Liu, E. Singer, W. Cohn, E. D. Micewicz, W. H. McBride, J. P. Whitelegge, J. A. Loo, *PROTEOMICS – Clin. Appl.* **2019**, 1900035.
- [6] V. K. Singh, T. M. Seed, *Int. J. Radiat. Biol.* **2017**, *93*, 851.
- [7] V. K. Singh, M. Garcia, T. M. Seed, *Int. J. Radiat. Biol.* **2017**, *93*, 870.
- [8] E. D. Micewicz, K. Kim, K. S. Iwamoto, J. A. Ratikan, G. Cheng, G. M. Boxx, R. D. Damoiseaux, J. P. Whitelegge, P. Ruchala, C. Nguyen, P. Purbey, J. Loo, G. Deng, M. E. Jung, J. W. Sayre, A. J. Norris, D. Schaeue, W. H. McBride, *PLoS One* **2017**, *12*, e0181577.
- [9] P. Teng, N. W. Bateman, B. L. Hood, T. P. Conrads, *J. Proteome Res.* **2010**, *9*, 6091.
- [10] H. M. Swartz, A. B. Flood, R. M. Gougelet, M. E. Rea, R. J. Nicolalde, B. B. Williams, *Health Phys.* **2010**, *98*, 95.
- [11] J. C. Silva, M. V Gorenstein, G.-Z. Li, J. P. C. Vissers, S. J. Geromanos, *Mol. Cell. Proteomics* **2006**, *5*, 144.
- [12] Y. Levin, E. Hradetzky, S. Bahn, *Proteomics* **2011**, *11*, 3273.

- [13] Y. Zhao, J. Yi, L. Tao, G. Huang, X. Chu, H. Song, L. Chen, *Cell Death Dis.* **2018**, 9, 433.
- [14] N. Cordes, J. Seidler, R. Durzok, H. Geinitz, C. Brakebusch, *Oncogene* **2006**, 25, 1378.
- [15] M. Sproull, K. Camphausen, *Radiat. Res.* **2016**, 186, 423.
- [16] D. Leszczynski, *Proteomics* **2014**, 14, 481.
- [17] Y.-B. Lim, B.-J. Pyun, H.-J. Lee, S.-R. Jeon, Y. B. Jin, Y.-S. Lee, *Proteomics* **2011**, 11, 1254.
- [18] O. Azimzadeh, M. J. Atkinson, S. Tapio, *Radiat. Environ. Biophys.* **2014**, 53, 31.
- [19] F. Marchetti, M. A. Coleman, I. M. Jones, A. J. Wyrobek, *Int. J. Radiat. Biol.* **2006**, 82, 605.
- [20] N. I. Ossetrova, D. J. Sandgren, W. F. Blakely, *Radiat. Prot. Dosimetry* **2014**, 159, 61.
- [21] S. Kulkarni, A. Koller, K. M. Mani, R. Wen, A. Alfieri, S. Saha, J. Wang, P. Patel, N. Bandeira, C. Guha, E. I. Chen, *Int. J. Radiat. Oncol.* **2016**, 96, 566.
- [22] S. D. Byrum, M. S. Burdine, L. Orr, S. G. Mackintosh, S. Authier, M. Pouliot, M. Hauer-Jensen, A. J. Tackett, *PLoS One* **2017**, 12, e0174771.
- [23] J. R. Whiteaker, L. Zhao, R. Saul, J. A. Kaczmarczyk, R. M. Schoenherr, H. D. Moore, C. Jones-Weinert, R. G. Ivey, C. Lin, T. Hiltke, K. W. Reding, G. Whiteley, P. Wang, A. G. Paulovich, *Radiat. Res.* **2018**, 189, 505.
- [24] D. R. Spitz, E. I. Azzam, J. Jian Li, D. Gius, *Cancer Metastasis Rev.* **2004**, 23, 311.
- [25] D. R. Spitz, M. Hauer-Jensen, *Antioxid. Redox Signal.* **2014**, 20, 1407.
- [26] M. Kobayashi, M. Yamamoto, *Antioxid. Redox Signal.* **n.d.**, 7, 385.

- [27] J.-M. Lee, J. Li, D. A. Johnson, T. D. Stein, A. D. Kraft, M. J. Calkins, R. J. Jakel, J. A. Johnson, *FASEB J.* **2005**, *19*, 1061.
- [28] T. W. Kensler, N. Wakabayashi, S. Biswal, *Annu. Rev. Pharmacol. Toxicol.* **2007**, *47*, 89.
- [29] M. Tsukimoto, N. Tamaishi, T. Homma, S. Kojima, *J. Radiat. Res.* **2010**, *51*, 349.
- [30] J. T. McDonald, K. Kim, A. J. Norris, E. Vlashi, T. M. Phillips, C. Lagadec, L. Della Donna, J. Ratikan, H. Szelag, L. Hlatky, W. H. McBride, *Cancer Res.* **2010**, *70*, 8886.
- [31] P. K. Purbey, P. O. Scumpia, P. J. Kim, A.-J. Tong, K. S. Iwamoto, W. H. McBride, S. T. Smale, *Immunity* **2017**, *47*, 421.
- [32] D. Murray, R. Mirzayans, W. H. McBride, *Radiat. Res.* **2018**, *190*, 331.
- [33] T. R. Knight, S. Choudhuri, C. D. Klaassen, *Toxicol. Sci.* **2007**, *100*, 513.
- [34] E. G. Wright, *Int. J. Radiat. Biol.* **2007**, *83*, 813.
- [35] J.-H. Kim, R. K. Thimmulappa, V. Kumar, W. Cui, S. Kumar, P. Kombairaju, H. Zhang, J. Margolick, W. Matsui, T. Macvittie, S. V Malhotra, S. Biswal, *J. Clin. Invest.* **2014**, *124*, 730.
- [36] J. P. Chute, *J. Clin. Invest.* **2014**, *124*, 960.
- [37] Y. Mohammed, A. J. Percy, A. G. Chambers, C. H. Borchers, *J. Proteome Res.* **2015**, *14*, 1137.
- [38] A. J. Percy, A. G. Chambers, D. S. Smith, C. H. Borchers, *J. Proteome Res.* **2013**, *12*, 222.
- [39] A. J. Percy, A. G. Chambers, J. Yang, D. B. Hardie, C. H. Borchers, *Biochim. Biophys. Acta - Proteins Proteomics* **2014**, *1844*, 917.

- [40] A. J. Percy, J. Yang, A. G. Chambers, R. Simon, D. B. Hardie, C. H. Borchers, *J. Proteome Res.* **2014**, *13*, 3733.
- [41] A. L. Oberg, O. Vitek, *J. Proteome Res.* **2009**, *8*, 2144.
- [42] M. Choi, C.-Y. Chang, T. Clough, D. Broudy, T. Killeen, B. MacLean, O. Vitek, *Bioinformatics* **2014**, *30*, 2524.
- [43] S. Rodrigues-Moreira, S. G. Moreno, G. Ghinatti, D. Lewandowski, F. Hoffschir, F. Ferri, A.-S. Gallouet, D. Gay, H. Motohashi, M. Yamamoto, M. C. Joiner, N. Gault, P.-H. Romeo, *Cell Rep.* **2017**, *20*, 3199.
- [44] D. E. Green, C. T. Rubin, *Bone* **2014**, *63*, 87.
- [45] S. C. Lu, *Mol. Aspects Med.* **2009**, *30*, 42.
- [46] J. Y. Chan, M. Kwong, *Biochim. Biophys. Acta - Gene Struct. Expr.* **2000**, *1517*, 19.
- [47] Y. Yang, Y. Chen, E. Johansson, S. N. Schneider, H. G. Shertzer, D. W. Nebert, T. P. Dalton, *Biochem. Pharmacol.* **2007**, *74*, 372.
- [48] Y. Chen, H. G. Shertzer, S. N. Schneider, D. W. Nebert, T. P. Dalton, *J. Biol. Chem.* **2005**, *280*, 33766.
- [49] D. M. Krzywanski, D. A. Dickinson, K. E. Iles, A. F. Wigley, C. C. Franklin, R. M. Liu, T. J. Kavanagh, H. J. Forman, *Arch. Biochem. Biophys.* **2004**, *423*, 116.
- [50] C. M. Krejsa, C. C. Franklin, C. C. White, J. A. Ledbetter, G. L. Schieven, T. J. Kavanagh, *J. Biol. Chem.* **2010**, *285*, 16116.
- [51] G. Ginsberg, S. Smolenski, D. Hattis, K. Z. Guyton, D. O. Johns, B. Sonawane, *J. Toxicol. Environ. Heal. Part B* **2009**, *12*, 389.
- [52] T. Wang, P. Arifoglu, Z. Ronai, K. D. Tew, *J. Biol. Chem.* **2001**, *276*, 20999.
- [53] S. G. Cho, Y. H. Lee, H. S. Park, K. Ryoo, K. W. Kang, J. Park, S. J. Eom, M. J.

- Kim, T. S. Chang, S. Y. Choi, J. Shim, Y. Kim, M. S. Dong, M. J. Lee, S. G. Kim, H. Ichijo, E. J. Choi, *J. Biol. Chem.* **2001**, 276, 12749.
- [54] A. Cholon, A. J. Giaccia, A. D. Lewis, I. Hickson, J. M. Brown, *Int. J. Radiat. Oncol. Biol. Phys.* **1992**, 22, 759.
- [55] K. J. Adams, J. Carmichael, C. R. Wolf, *Cancer Res.* **1985**, 45, 1669.
- [56] S. T. Fraser, R. G. Midwinter, B. S. Berger, R. Stocker, *Adv. Hematol.* **2011**, 2011, 473709.
- [57] S. T. Fraser, R. G. Midwinter, B. S. Berger, R. Stocker, *Adv. Hematol.* **2011**, 2011, 473709.
- [58] L. E. Otterbein, A. Hedblom, C. Harris, E. Csizmadia, D. Gallo, B. Wegiel, *Proc. Natl. Acad. Sci. U. S. A.* **2011**, 108, 14491.
- [59] B. Halliwell, J. M. C. Gutteridge, *Free Radicals in Biology and Medicine*, Oxford University Press, **2015**.
- [60] N. Mori, M. Okumoto, M. Yonezawa, R. Nishikawa, Y. Takamori, K. Esaki, *J. Radiat. Res.* **1994**, 35, 1.
- [61] H. I. Kohn, R. F. Kallman, *Radiat. Res.* **1956**, 5, 309.
- [62] T. H. Roderick, *Radiat. Res.* **1963**, 20, 631.
- [63] C. Chen, S. A. Lorimore, C. A. Evans, A. D. Whetton, E. G. Wright, *Proteomics* **2005**, 5, 4254.
- [64] P. J. Coates, J. K. Rundle, S. A. Lorimore, E. G. Wright, **2008**, DOI 10.1158/0008-5472.CAN-07-3050.
- [65] J. P. Williams, S. L. Brown, G. E. Georges, M. Hauer-Jensen, R. P. Hill, A. K. Huser, D. G. Kirsch, T. J. Macvittie, K. A. Mason, M. M. Medhora, J. E. Moulder, P.

- Okunieff, M. F. Otterson, M. E. Robbins, J. B. Smathers, W. H. McBride, *Radiat. Res.* **2010**, *173*, 557.
- [66] R. Stojković, A. Fucic, D. Ivanković, Z. Jukić, P. Radulović, J. Grah, N. Kovačević, L. Barišić, B. Krušlin, *Arch. Ind. Hyg. Toxicol.* **2016**, *67*, 297.
- [67] I. Pogribny, J. Raiche, M. Slovack, O. Kovalchuk, *Biochem. Biophys. Res. Commun.* **2004**, *320*, 1253.
- [68] Y. Ilnytsky, F. J. Zemp, I. Koturbash, O. Kovalchuk, *Biochem. Biophys. Res. Commun.* **2008**, *377*, 41.
- [69] N. R. Jog, R. Caricchio, *Cell Death Dis.* **2013**, *4*, e758.
- [70] W.-L. Hsu, D. L. Preston, M. Soda, H. Sugiyama, S. Funamoto, K. Kodama, A. Kimura, N. Kamada, H. Dohy, M. Tomonaga, M. Iwanaga, Y. Miyazaki, H. M. Cullings, A. Suyama, K. Ozasa, R. E. Shore, K. Mabuchi, *Radiat. Res.* **2013**, *179*, 361.
- [71] N. L. Anderson, N. G. Anderson, L. R. Haines, D. B. Hardie, R. W. Olafson, T. W. Pearson, *J. Proteome Res.* **2004**, *3*, 235.
- [72] A. Mateus, T. A. Määttä, M. M. Savitski, *Proteome Sci.* **2016**, *15*, 13.
- [73] D. Martinez Molina, R. Jafari, M. Ignatushchenko, T. Seki, E. A. Larsson, C. Dan, L. Sreekumar, Y. Cao, P. Nordlund, *Science* **2013**, *341*, 84.
- [74] M. M. Savitski, F. B. M. Reinhard, H. Franken, T. Werner, M. F. Savitski, D. Eberhard, D. M. Molina, R. Jafari, R. B. Dovega, S. Klaeger, B. Kuster, P. Nordlund, M. Bantscheff, G. Drewes, *Science* **2014**, *346*, 1255784.
- [75] H. Franken, T. Mathieson, D. Childs, G. M. A. Sweetman, T. Werner, I. Tögel, C. Doce, S. Gade, M. Bantscheff, G. Drewes, F. B. M. Reinhard, W. Huber, M. M.

- Savitski, *Nat. Protoc.* **2015**, *10*, 1567.
- [76] M. Schenone, V. Dančik, B. K. Wagner, P. A. Clemons, *Nat. Chem. Biol.* **2013**, *9*, 232.
- [77] M. Gaetani, P. Sabatier, A. A. Saei, C. Beusch, Z. Yang, S. Lundström, R. A. Zubarev, *bioRxiv* **2018**, 496398.
- [78] M. M. Savitski, T. Mathieson, N. Zinn, G. Sweetman, C. Doce, I. Becher, F. Pachi, B. Kuster, M. Bantscheff, *J. Proteome Res.* **2013**, *12*, 3586.
- [79] I. Neganova, F. Vilella, S. P. Atkinson, M. Lloret, J. F. Passos, T. von Zglinicki, J.-E. O'Connor, D. Burks, R. Jones, L. Armstrong, M. Lako, *Stem Cells* **2011**, *29*, 651.
- [80] H.-H. Li, Y.-W. Wang, R. Chen, B. Zhou, J. D. Ashwell, A. J. Fornace, Jr., *Int. J. Biol. Sci.* **2015**, *11*, 726.
- [81] M. G. Alexandrow, J. L. Hamlin, *J. Cell Biol.* **2005**, *168*, 875.
- [82] J. Bednar, I. Garcia-Saez, R. Boopathi, A. R. Cutter, G. Papai, A. Reymer, S. H. Syed, I. N. Lone, O. Tonchev, C. Crucifix, H. Menoni, C. Papin, D. A. Skoufias, H. Kurumizaka, R. Lavery, A. Hamiche, J. J. Hayes, P. Schultz, D. Angelov, C. Petosa, S. Dimitrov, *Mol. Cell* **2017**, *66*, 384.
- [83] E. M. Yazlovitskaya, P. A. Voziyan, T. Manavalan, W. G. Yarbrough, A. V Ivanova, *Cell Death Dis.* **2015**, *6*, e1652.
- [84] E. M. Yazlovitskaya, R. Uzhachenko, P. A. Voziyan, W. G. Yarbrough, A. V Ivanova, *Cell Death Dis.* **2013**, *4*, e687.
- [85] E. I. Azzam, J.-P. Jay-Gerin, D. Pain, *Cancer Lett.* **2012**, *327*, 48.